

AFOSR-TR-8697

0064

**DISTRIBUTION STATEMENT A**

Approved for public release  
Distribution Unlimited



**CERAMICS DIVISION**  
**MATERIALS SCIENCE AND ENGINEERING**  
University of Illinois  
Urbana, Illinois

DTIC QUALITY INSPECTED 1

REPORT DOCUMENTATION PAGE			Form Approved OMB No. 0704-0188	
Public reporting burden for this collection of information is estimated to average 1 hour per response, including the time for reviewing instructions, searching existing data sources, gathering and maintaining the data needed, and completing and reviewing the collection of information. Send comments regarding this burden estimate or any other aspect of this collection of information, including suggestions for reducing this burden, to Washington Headquarters Services, Directorate for Information Operations and Reports, 1215 Jefferson Davis Highway, Suite 1204, Arlington, VA 22202-4302, and to the Office of Management and Budget, Paperwork Reduction Project (0704-0188), Washington, DC 20503.				
1. AGENCY USE ONLY (Leave blank)	2. REPORT DATE Dec. 5, 1996	3. REPORT TYPE AND DATES COVERED Final Report for Apr. 1, 1993 to Mar. 30		
4. TITLE AND SUBTITLE Transformation Weakening of Ceramic Composite Interfaces		5. FUNDING NUMBERS AFOSR F49620-93-1-0227		
6. AUTHOR(S) Professor Waltraud M. Kriven				
7. PERFORMING ORGANIZATION NAME(S) AND ADDRESS(ES) University of Illinois at Urbana-Champaign Dept. of Materials Science and Engineering 1304 W. Green St. Urbana, IL 61801		8. PERFORMING ORGANIZATION REPORT NUMBER		
9. SPONSORING/MONITORING AGENCY NAME(S) AND ADDRESS(ES) AFOSR/NC, Division of Chemistry and Materials Science 110 Duncan Ave., Suite B115 Bolling AFB, DC 20332-0001		10. SPONSORING/MONITORING AGENCY REPORT NUMBER		
11. SUPPLEMENTARY NOTES				
12a. DISTRIBUTION/AVAILABILITY STATEMENT  Public availability		12b. DISTRIBUTION CODE		
13. ABSTRACT (Maximum 200 words) Phase stability and transformations in some chosen ceramics was investigated and several new transformations in oxide systems were identified. To quantitatively understand the coupling of mechanical shear stress to nucleation, a constrictive double shear test was devised. It indicated that a minimum debonding shear strength of 95 MPa was needed to overcome the nucleation barrier for the proto (orthorhombic) to clino (monoclinic) transformation in enstatite ( $\text{MgO} \cdot \text{SiO}_2$ ) and to give rise to "transformational plasticity" in the polycrystalline ceramic. For comparison with transformation weakening, monazite ( $\text{LaPO}_4$ ) and zenotime ( $\text{YPO}_4$ ) fiber coatings were studied. Fiber pushout measurements indicated debonding shear strengths of 110-120 MPa were required for $\text{LaPO}_4$ coatings, versus 95 MPa for $\text{YPO}_4$ , depending on coating thickness. A four layer, strong and damage tolerant oxide laminate was devised, based on $\text{YPO}_4$ , yttria stabilized zirconia (3 mol% $\text{Y}_2\text{O}_3\text{-ZrO}_2$ ) and alumina ( $\text{Al}_2\text{O}_3$ ), and having four point bend strengths of ~392 MPa and work of fracture of ~10 $\text{KJm}^{-2}$ . Amorphous mullite ( $3\text{Al}_2\text{O}_3 \cdot \text{SiO}_2$ ) and YAG ( $\text{Y}_3\text{Al}_5\text{O}_{12}$ ) fibers of tensile strengths 6.0 and 2.4 GPa respectively, were collaboratively fabricated and evaluated. Transformation weakening was demonstrated as a viable mechanism for interphase debonding in oxide systems. $\text{YPO}_4$ demonstrated chemical compatibility in air with YAG ( $\text{Y}_3\text{Al}_5\text{O}_{12}$ ) and mullite ( $3\text{Al}_2\text{O}_3 \cdot \text{SiO}_2$ ) up to temperatures of 1600°C and 1500°C, respectively.				
14. SUBJECT TERMS Transformation weakening, transformational plasticity, constrictive double shear test, fiber pushout, monazite or zenotime coatings, mullite fibers, debonding shear strengths		15. NUMBER OF PAGES 77		
		16. PRICE CODE		
17. SECURITY CLASSIFICATION OF REPORT	18. SECURITY CLASSIFICATION OF THIS PAGE	19. SECURITY CLASSIFICATION OF ABSTRACT	20. LIMITATION OF ABSTRACT	

# TRANSFORMATION WEAKENING OF CERAMIC COMPOSITE INTERFACES

A final research report for grant number  
F49620-93-1-0227

FINAL REPORT  
For the period April 1st 1993 to March 30th 1996

Dec 6th 1996

Prepared for:  
Dr. Alexander Pechenik  
Program Manager,  
Directorate of Chemistry and Materials Science,  
AFOSR  
110 Duncan Ave, Suite B115,  
Bolling Air Force Base, DC 20332-0001

Prepared by:  
The University of Illinois at Urbana-Champaign,  
Department of Materials Science and Engineering,  
1304 West Green St., Urbana, IL 61801

Principal Investigator  
Professor Waltraud M. Kriven

19970128 185

## Table of Contents

Section 1. Introduction and Overall Objectives .....	3
2. Accomplishments .....	7
3. Personnel Supported .....	16
4. Publications .....	17
5. Interactions/Transitions .....	22
6. New Discoveries, Inventions or Patents .....	30
7. Honors/Awards .....	31
8. Synopsis of Theses .....	32

## SECTION I INTRODUCTION AND OVERALL OBJECTIVES

### Introduction to transformation weakening of interfaces

The concept of "phase transformation weakening" introduced by Professor Kriven has led to the search for a displacive or martensitic phase transformation with a negative volume change or large shape change at fiber/matrix or laminate/matrix interfaces (see Table 1). Several materials are considered to be promising candidates as "phase transformation weakeners". Preliminary studies have been conducted on enstatite ( $\text{MgO} \cdot \text{SiO}_2$  or  $\text{MgSiO}_3$ ), which is accompanied by a 5.5 % volume contraction on transformation. In applying such a phase transformation, a distinction is drawn between a thermally induced transformation and a shear stress induced transformation. Figure 1 illustrates a mechanism for shear stress induced weakening of an interface and thereby, overall toughening of a composite. The difference between a shear induced mechanism and a thermally induced one is that in the latter, all the interfacial grains have already been transformed prior to crack approach.

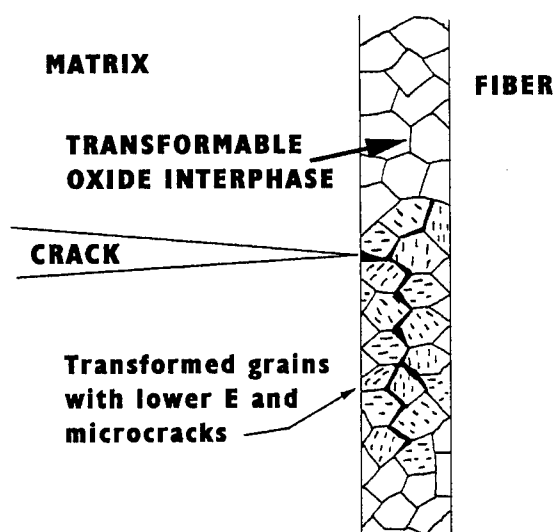


Fig. 1 Schematic diagram illustrating "transformation weakening of ceramic interphases" leading to overall toughening of a ceramic matrix composite. In thermally induced transformations, all interphases are pre-transformed before the approach of a crack with some consequent loss of overall strength of the material. In the ideal shear-stress induced case, an on-coming crack induces a transformation in its immediate environment, with strength only minimally reduced throughout the bulk. Maximum toughening is achieved since the propagating crack need to do work to overcome the nucleation barrier and cause transformation, and onset of the other synergistic toughening mechanisms occurs.

The main features and potential advantages of transformation weakened interfaces can be summarized as follows.

- (1) An oxide coating at interfaces between oxide fibers embedded in an oxide matrix or in a laminated composite will allow chemical stability in a oxidizing environment.
- (2) Strong bonding, and hence good overall strength of the composite, can be switched to weak bonding in the *localized* region of an incoming crack when the shear stresses associated with the crack-fiber or laminate interface induce a transformation in the coating. Thus the interface strength can be varied as it exhibits "dynamic" interfacial properties (i.e., it could be described as "smart" or "adaptive"). Unlike the current generation of fiber reinforced composites, the strength does not need to be sacrificed to improve the toughness.
- (3) It is possible to design a composite with a single crystal oxide fiber and an oxide matrix of the same chemical composition, such that the transformation weakener is adjacent to that composition on the equilibrium phase diagram. Then one could minimize the thermal expansion mismatch ( $\Delta\alpha$ ) problem and eliminate the high temperature chemical reaction ( $\Delta G_{\text{chem}}$ ) problem.

The potential energy dissipative mechanisms are many fold:

- (i) They involve using crack energy to nucleate the phase transformation.
- (ii) This may also cause autocatalytic nucleation of transformation along the interface promoting long fiber pullout or interfacial debonding.
- (iii) There is an increased surface energy contribution with interfacial microcracking or shearing accompanying the transformation.
- (iv) Increased frictional work needs to be done by the crack to achieve interfacial debonding, so that there is a need to optimize coating thickness to achieve an optimum process zone.

Table 1. Examples of First Order Displacive Transformations in Ceramics

<u>Compound</u>	<u>Crystal Symmetries</u>	<u>Transformation Temperature</u> <u>(T<sub>0</sub> on cooling)</u>	<u>Volume Change</u> <u>(<math>\Delta V</math>)</u>	<u>Unit Cell Shape Change(°)</u>
ZrO <sub>2</sub>	tetragonal → monoclinic	950	(+)4.9% (R.T.)	9
Ln <sub>2</sub> O <sub>3</sub> (type)	monoclinic → cubic	600–2200	(+)10%	10
Ca <sub>2</sub> SiO <sub>4</sub> (K <sub>2</sub> SO <sub>4</sub> -type)	monoclinic → orthorhombic	490	(+)12%	4.6
Sr <sub>2</sub> SiO <sub>4</sub> (K <sub>2</sub> SO <sub>4</sub> -type)	orthorhombic → monoclinic	90	0.2%	2
NiS	rhombohedral → hexagonal	379	(+)4%	—
2Tb <sub>2</sub> O <sub>3</sub> .Al <sub>2</sub> O <sub>3</sub> (type)	orthorhombic → monoclinic	1070	(+)0.67%	18.83
PbTiO <sub>3</sub>	cubic → tetragonal	445	(+)1%	0
KNbO <sub>3</sub>	tetragonal → orthorhombic	225	~0%	0
LuBO <sub>3</sub>	hexagonal → rhombohedral	1310	(+)8%	—
MgSiO <sub>3</sub> (CaSiO <sub>3</sub> -type) (FeSiO <sub>3</sub> -type)	orthorhombic → monoclinic	865	(-)5.5%	18.3
YNbO <sub>4</sub> (LnNbO <sub>4</sub> -type)	tetragonal → monoclinic	900	(-) 1.8%	4.53
LnBO <sub>3</sub> (type)	hexagonal → hexagonal	550–800	(-)8.2%	—

Thus, fiber/matrix interfaces in ceramic matrix composites must be sufficiently strong to provide for mechanical integrity of the composites, but also weak enough to prevent transition of cracks from matrix to fibers. This project explores a fundamentally new concept of a "variable-strength" interface, viz., one that is strong when no cracks are present, but suddenly weakens and arrests the propagation of a crack when it arrives near such an interface. The effect is produced by coating ceramic fibers with a thin layer of a ceramic material capable of quick, stress-induced transformation with a negative volume change and/or a large unit cell shape change.

### Overall Objectives

Thus, the objective of this work was to investigate a novel concept for developing superior fiber-matrix interfaces in ceramic matrix composites by utilizing the "transformation weakening effect." Since many of the transformable phases are oxides, this work opens the door to high temperature, oxidation resistant composites. The proposed transformation weakening mechanism for toughening of fiber-reinforced, oxide, ceramic composites is illustrated in Fig. 1.

In this work the concept would be tested on model diffusion couples and in dense, machined cylinders embedded in a matrix, to represent fiber/matrix interfaces in fiber reinforced composites. The fundamentals of the transformation are investigated on the model systems using microstructure characterization techniques of XRD, SEM, TEM, HVEM and HREM, to measure the amount of transformed material.

Fibers were to be coated with the selected transformable ceramic coating, and the composites produced are tested for interfacial strength and fracture by a fiber-push test. Vickers indentation tests would be performed and bulk mechanical properties of strength and work of fracture are determined. Fibrous and laminated composite configurations were planned for bulk mechanical evaluation of promising transformable composite materials.



## SECTION 2. ACCOMPLISHMENTS

The accomplishments reported here are summarized in the 35 journal papers, 5 conference proceedings published and submitted, and 7 publications in preparation, as well as 13 invited talks and 47 conference presentations listed in Section 4. In addition applications for two patents are in progress. The publications are grouped in sub-topics which can be described as follows.

### *Phase Transformations*

In the area of phase transformations, the basic science of phase stability and phase transformations in some chose ceramic systems were investigated. Known transformations in ceramics and mineral systems for which ceramic analogies could be synthesized have been surveyed. It was found that knowledge about the existence of phase transformations at high temperatures (e.g. above 1000°C) was significantly lacking. Several new transformations were added to the list of known or suspected systems, as illustrated in Table 2. This review is useful as a starting point in assessing the potential contributions of phase transformations in structural ceramic composites. These applications lie in:

- (i) Transformation toughening of ceramic matrix composites
- (ii) Transformation weakening of critical interphases in composites,
- (iii) Energy dissipation by ferroelastic domain rearrangements
- (iv) Large force actuators

An effort was made to concentrate on forefront research in oxide ceramics rather than on non-oxide materials, since only materials which can maintain their chemically stability at elevated temperatures in an oxidizing environment will be of long term use in some of the most severe operating conditions.

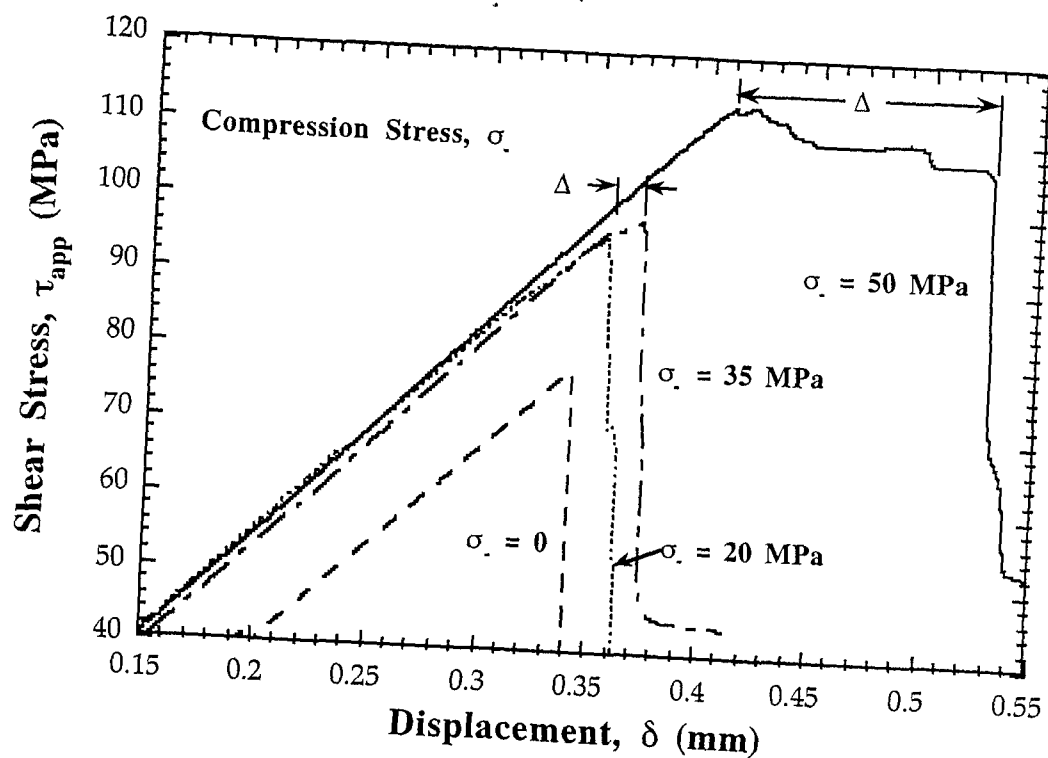
### *Shear-induced Nucleation*

In the nucleation of phase transformations is a poorly understood area, especially the nucleation of martensitic transformations. Due to the ambiguity in ductile metals of dislocation formation causing nucleation or vice versa, (a chicken or egg argument), the phase transformations community is looking towards ceramics to gain a better understanding of nucleation. In ceramics dislocations rarely form on deformation, and so the ambiguity is removed. Current theories in physics discuss solitons and localized soft modes, but there are few definitive experiments in this area. To better understand the coupling of mechanical shear stress to nucleating a

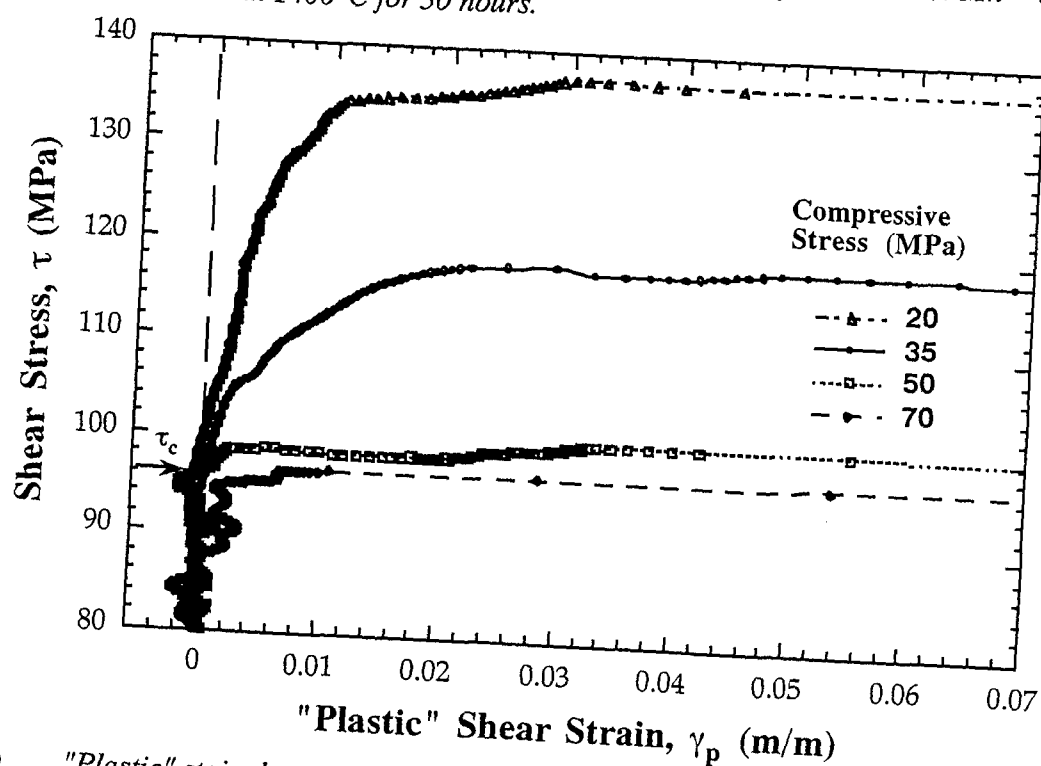
phase transformation, we have devised a "constrictive double shear test." In this test a polycrystalline flexure specimen is subjected to essentially mode II shear while in a state of compression so as to surpass the tensile strength of the polycrystalline ceramic. The critical shear to induce transformation is thus measured as the ceramic exhibits "plasticity" in its stress *vs* strain curve, as illustrated in Fig 2. The double shear test is a model system to probe the behavior of a polycrystalline ceramic coating at a fiber-matrix interphase where large shear forces are anticipated to exist during fracture of the composite.

**Table 2. Other Examples of Phase Transformations in Ceramics**

<u>Compound</u>	<u>Crystal Symmetries</u>	<u>Transformation Temperature (T<sub>0</sub> on cooling)</u>	<u>Volume Change (<math>\Delta V</math>)</u>	<u>Unit Cell Shape Change(°)</u>
Cristobalite (SiO <sub>2</sub> )	cubic → tetragonal	265	(-) 2.8%	0
Hexacelcian (BaAl <sub>2</sub> Si <sub>2</sub> O <sub>8</sub> )	hexagonal → orthorhombic	300	(-) 0.43%	0
Leucite (KAlSi <sub>2</sub> O <sub>6</sub> )	cubic → tetragonal	620	~0	0
Zircon (ZrSiO <sub>4</sub> )	monoclinic → tetragonal	827	?	?
Di-lanthanide aluminates (Ln <sub>4</sub> Al <sub>2</sub> O <sub>9</sub> )	monoclinic → monoclinic	1400	(+) 0.5%	?
Di-lanthanide titanates (Ln <sub>2</sub> TiO <sub>5</sub> )	hexagonal → orthorhombic	1712	?	0
Barium orthotitanate (Ba <sub>2</sub> TiO <sub>4</sub> )	?	?	?	?
Cerium pyrosilicate (CeSiO <sub>4</sub> )	?	?	?	?
Aluminum titanate (Al <sub>2</sub> TiO <sub>5</sub> )	?	?	?	?
Lithium phosphate (Li <sub>2</sub> PO <sub>4</sub> )	?	340	?	?
Lanthanide (eg.Gd) vanadates (LnVO <sub>4</sub> )	monoclinic → tetragonal	825	?	?



(a) Applied shear stress - displacement curves for  $\text{MgSiO}_3$  with 2 mol%  $\text{Mn}^{2+}$  dopant as sintered at  $1400^\circ\text{C}$  for 30 hours.



(b) "Plastic" stain due to transformation in  $\text{MgSiO}_3$  with 2 mol%  $\text{Mn}^{2+}$  dopant,  $\tau_c$  indicates the critical shear stress of transformation.

Fig.2 Stress vs strain curves of double shear tests.

### *Coatings*

In order to study the behavior of transformation weakeners as fiber/matrix interphases, it was necessary to deposit suitable oxides as coatings on fibers. The standard procedure of dip coating did not always yield a regular cylindrical shape as some coating grains tended to diffuse into the matrix forming a halo. A new technique for depositing dense, amorphous layers of oxide of well defined thickness and chemical composition was developed. Pulsed eximer laser ablation (PELA) of a target oxide pellet was able to produce a smooth dense coating of the precise stoichiometry as the target material. This was the first time that the relatively new PELA technique was applied to fiber coating and it was found to be relatively successful. The technique was further studied in the production and characterization of nano crystalline, nanolaminates of niobium aluminide and aluminum ( $\text{NbAl}_3/\text{Al}$ ).

### *Monazite ( $\text{LaPO}_4$ ) and Zenotime ( $\text{YPO}_4$ ) Interfaces*

During the period of this research the rare earth phosphates ( $\text{LnPO}_4$ ) were hailed as suitable high temperature interphase materials for oxide composites. The debonding was proposed to occur by a simple slippage mechanism. However, controversy existed about the chemical stability of monazite if the fiber coating solution was not exactly stoichiometric. Our research in the  $\text{LaPO}_4$  and  $\text{Al}_2\text{O}_3$  system concurred with this finding, which led us to propose the use of zenotime instead of monazite, since yttria behaved as a lanthanide element but lacked the  $4f$  orbital electrons and so less readily formed compounds.  $\text{YPO}_4$  was found to be chemically stable with yttrium aluminate garnet (YAG, or  $\text{Y}_3\text{Al}_5\text{O}_{12}$ ) up to  $1600^\circ\text{C}$  in air, as well as with yttria stabilized zirconia (3Y-TZP).

### *Interface Property Measurements by Fiber Pushout Testing*

In order to determine the effectiveness of transformation weakeners leading to debonding, a fiber pushout apparatus was designed and built. It was superior to many other current models in having precise control of the punch by *in situ* double X-Y positioning tables. The apparatus was used to measure pushout of SiC fibers (Textron SCS-6) coated with graphite in a SiAlON matrix and monazite ( $\text{LaPO}_4$ ) or zenotime ( $\text{YPO}_4$ ) coated alumina and YAG fibers. The data was analyzed using the various models including simple shear, shear lag, progressive debonding, and the Liang and Hutchinson models. The latter was found to be the most rigorous. In the case of the phosphate coatings of systematically varying thickness, the good match between

theory and experiment for the  $\text{YPO}_4$  / YAG system *vs* a poor match for the  $\text{LaPO}_4$  /  $\text{Al}_2\text{O}_3$  system confirmed that chemical degradation occurred with monazite at high densification temperatures.

Several interface debonding parameters were measured by the fiber pushout test, including:

- (i) interface fracture energy ( $\Gamma_{\text{II}}$ ) in  $\text{J/m}^2$
- (ii) coefficient of friction ( $\mu$ )
- (iii) clamping stress ( $\sigma_{\text{clamping}}$ ) in MPa
- (iv) average residual axial stress in MPa
- (v) average residual radial stress in MPa
- (vi) asperity pressure ( $\sigma_{\text{asperity}}$ ) in MPa
- (vii) interface debond stress ( $\tau_d$ ) in MPa
- (viii) interface frictional stress ( $\tau_f$ ) in MPa

However, for purposes of comparison the debonding shear strength ( $\tau_d$ ) was measured for several different systems, and the current status of comparison among different debonding systems is presented in Table 3.

**Table 3. Comparison of debonding mechanisms**

System	Debonding mechanism	Debonding shear strength ( $\tau_d$ ) MPa
SiC fiber / C coating	interface slippage	10 - 15
$\text{Al}_2\text{O}_3$ fiber / $\text{LaPO}_4$ coating	interface slippage	110 - 120
YAG fiber / $\text{LaPO}_4$ coating		F(thickness)
YAG fiber / $\text{YPO}_4$ coating	interface slippage	95
		F(thickness)
PE $\rightarrow$ PE transformation in enstatite ( $\text{MgO} \cdot \text{SiO}_2$ )	transformation weakening	95
$\beta \rightarrow \alpha$ transformation in cristobalite ( $\text{SiO}_2$ )	transformation weakening	in progress
( $\text{Al}_2\text{O}_3$ fiber / $\text{K}_2\text{CaNb}_2\text{O}_7$ powder	cleavage planes	in progress

#### *Oxide Laminates*

Since chemically compatible oxide fibers were not available for the transformation weakened coating systems, multilayered oxide laminates were fabricated by tape casting as model systems for studying interphase behavior. To obtain experience with the mechanical behavior of laminates for comparison with laminates containing transformation weakened interphases, three kinds of multiplayer

laminates were fabricated: simple two layer laminates, laminates with different configurations, and  $\text{ZrO}_2 / \text{Al}_2\text{O}_3$  laminates separated by  $\text{YPO}_4$  or  $\text{LaPO}_4$ . The work has been comprehensively written up in the Ph. D. thesis of Dong Hau Kuo, a synopsis of which is attached.

One of the highlights of this work is that for the first time a strong and damage tolerant oxide composite has been fabricated. Specifically, a four-layered configuration of  $\text{YPO}_4 / 3\text{Y-ZrO}_2 / 30 \text{ vol}\% 3\text{Y-ZrO}_2$  in  $70 \text{ vol}\% \text{Al}_2\text{O}_3 / 3\text{Y-ZrO}_2$  was fabricated in which  $\text{YPO}_4$  was the weak interphase layer. Two composites were fabricated which yielded un-notched, four-point bend strengths of 358 and 392 MPa and apparent work-of-fracture values of 8.2 and 10  $\text{KJ/m}^2$ , respectively, as seen in Figs 3(a). Extensive delamination indicating significant energy dissipative mechanisms are evidenced in the SEM micrograph of Fig. 3(b). Other transformation weakened laminates have also been examined and will be reported at a latter date when a patent has been filed.

#### *Fiber-reinforced SiAlON Composites*

Early on in this work, it was considered to be beneficial to gain some experience with currently functional fiber-reinforced composites. The system chosen was a SiAlON matrix reinforced with commercially available silicon carbide (SiC, Textron SCS-6) fibers coated with  $6 \mu\text{m}$  of carbon. The bulk stress vs strain curves and debonding mechanisms were examined for a full understanding of fiber bridging mechanisms, and to give guidance in the design of oxide composites. This work was primarily carried out by Dr. Chao Huang, who obtained employment at the Energy research Corporation. Subsequently Dr. Chao externally continued his collaboration with our group at UIUC, and hence a large number of publications in this area resulted.

**Load vs Displacement Curves of a  $\text{YPO}_4/\text{Y-ZrO}_2/30 \text{ vol\% Y-ZrO}_2\text{-}70 \text{ vol\% Al}_2\text{O}_3/\text{Y-ZrO}_2$  Laminate Tested in 4-Point Flexure**

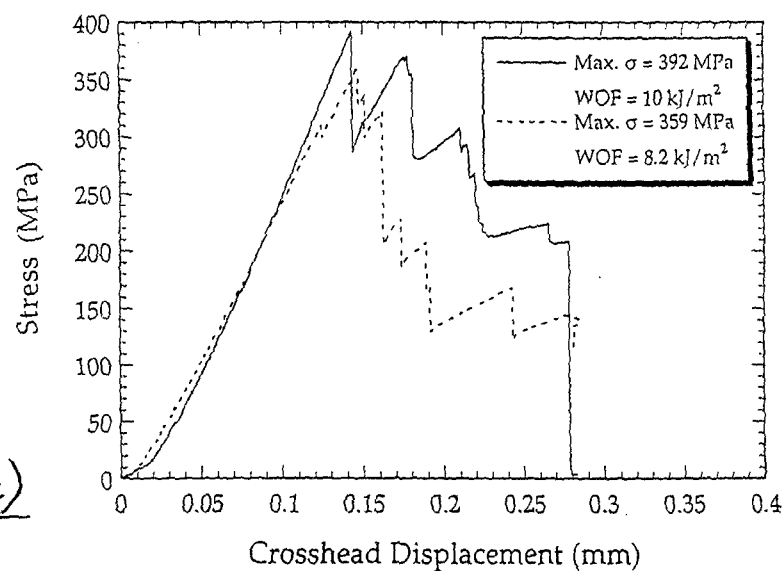


Fig. 3(a)

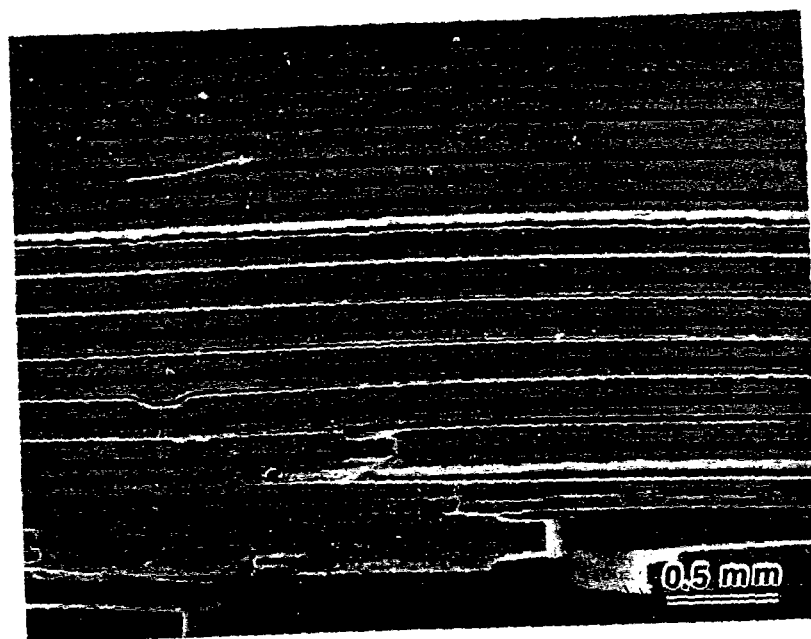


Fig. 3(b) Scanning electron microscopy, side view of a  $\text{YPO}_4/\text{Y-ZrO}_2/30 \text{ vol\% Y-ZrO}_2\text{-}70 \text{ vol\% Al}_2\text{O}_3/\text{Y-ZrO}_2$  oxide laminate tested in four-point bending. Pronounced interfacial delamination occurred in the bottom half of the bar, which was under tensile loading, while the top half, which was under compressive loading, remained intact.

### *Oxide Fibers*

In view of the crucial need for oxide fibers collaborative work was undertaken with the Containerless Research Inc. company in Chicago, IL with some modest stage I funding for six months under a stage I SBIR. The personnel supported on this AFOSR also worked in the microstructural characterization and mechanical evaluation of mullite ( $3\text{Al}_2\text{O}_3 \cdot 2\text{SiO}_2$ ) and YAG ( $\text{Y}_3\text{Al}_5\text{O}_{12}$ ) fibers.

Fibers were pulled from undercooled melts and at high pulling rates, which results in cooling rates in excess of  $1000^\circ\text{C}/\text{s}$  in the region just outside the liquid source. Crystallization is suppressed and glass fibers are formed. In order to pull fibers, it was necessary to pull at a rate greater than the crystallization velocity of the undercooled liquid from which the fibers are being pulled. If this condition is not met, the undercooled liquid will crystallize. The need for fast pulling to avoid crystallization of the drop makes the process inherently fast with pulling rates greater than  $1 \text{ m/s}$  for  $20 \mu\text{m}$  diameter fibers. The production rate compares favorably with the pedestal growth and edge-defined, film-fed growth techniques which provide *ca.*  $100 \mu\text{m}$  diameter crystalline fibers grown at much slower rates.

Fibers coated with yttrium phosphate and embedded in a mullite matrix retained their shape during the  $1500^\circ\text{C}$  sintering process. This result shows that these materials have good potential for use in high temperature applications.

Microstructural analysis shows that the fibers had a smooth and homogeneous surface (Fig.4). The tensile strength of the amorphous  $3\text{Al}_2\text{O}_3 \cdot 2\text{SiO}_2$  fibers was *ca.*  $6 \text{ GPa}$  which significantly exceeds the *ca.*  $2.1 \text{ GPa}$  strength of commercially available fine grained alumina fibers (Nextel 720). Alumino-silicate fibers of the  $3\text{Al}_2\text{O}_3 \cdot 2\text{SiO}_2$  mullite composition were crystallized at  $1200^\circ\text{C}$  into random orientations and sub-micron grain size. Their tensile strength was of the order of  $1 \text{ GPa}$ . This method of crystallization by heating the whole fiber at once, at the annealing temperature, yielded a microstructure which suggested that nucleation occurred at multiple sites and in an uncontrolled way. Future work is planned in which the fibers will be directionally annealed to achieve control of nucleation and growth and perhaps obtain crystallographic alignment within the fiber.

The crystal structures of mullite ( $3\text{Al}_2\text{O}_3 \cdot 2\text{SiO}_2$ ) and the high pressure sillimanite ( $\text{Al}_2\text{O}_3 \cdot \text{SiO}_2$ ) polymorph on which it is based basically consist of chain structures of edge-shared  $\text{AlO}_6$  octahedra arranged parallel to the



orthorhombic [c] axis, and placed at the corners and center of each unit cell. In sillimanite, there are a further four chains of alternating  $\text{AlO}_4$  and  $\text{SiO}_4$  corner-shared tetrahedra which are arranged symmetrically within the unit cell. In mullite, only three chains of  $\text{AlO}_4/\text{SiO}_4$  tetrahedra are arranged within each unit cell so as to be statistically randomized to X-ray diffraction, but give rise to the complex incommensurate modulations observed by TEM. Thus extremely high strength and creep resistance would be expected from single crystal fibers having the [c] axis aligned parallel to the fiber length. One may speculate that even a polycrystalline, textured fiber with aligned [c] axes should yield significantly improved tensile strengths, as compared to randomly crystallized polycrystalline fibers.

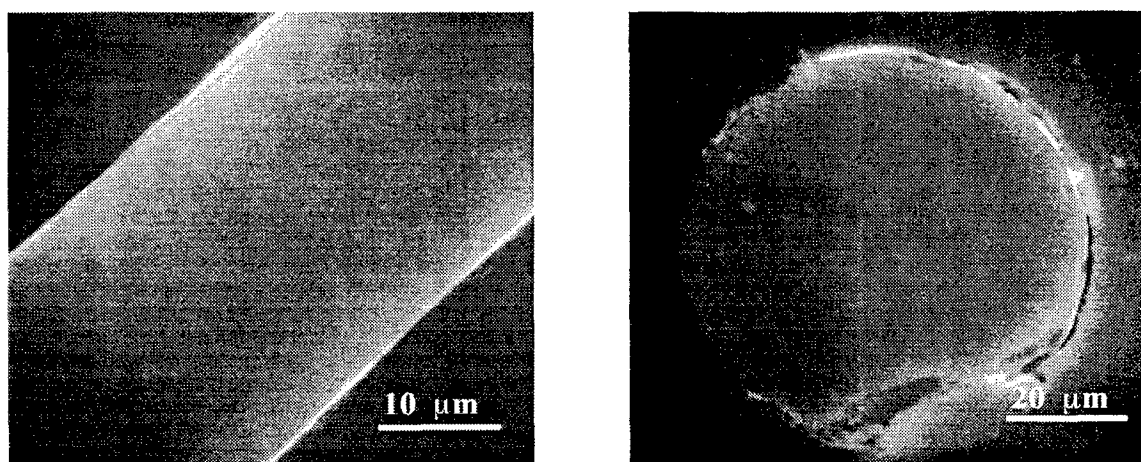


*Fig. 4 SEM of a 3:2 mullite fiber. The fiber surface was smooth, homogeneous and free from imperfections. The fiber was pulled in oxygen from a drop of liquid undercooled to ca. 1675 K; (a) fiber surface (b) fiber cross section.*

Thus oxide glass fibers with fracture strengths up to 6 GPa can reproducibly be made by pulling from undercooled molten oxide precursors. Glass fibers (e.g. mullite, YAG) can be recrystallized to form equilibrium phases corresponding to the composition of the starting material. Alumino-silicates of the  $3\text{Al}_2\text{O}_3 \cdot 2\text{SiO}_2$  composition crystallize into the equilibrium 3:2 mullite form.

### SECTION 3. PERSONNEL SUPPORTED

- Professor Waltraud M. Kriven PI (1 summer month per annum)
- Dr. Chao M. Huang, processing and mechanical testing expert, supported on this project for 2 years.
- Dr. Mohammad H. Jilavi, TEM expert was entirely supported for one year starting on March 20th 1995.
- Dr. Dong Zhu, mechanical testing expert was partially supported on this grant for two years, and for six months on an AFOSR SBIR with Containerless Research Incorporated.
- Mr. Dong Hau Kuo, Ph. D. student had a 50% teaching assistantship, for three semesters, as was supported for two years on this AFOSR grant.
- Dr. Sang Jin Lee, processing expert, visiting scientist with partial funding for living expenses, from Korea. Supplemented his salary at \$10,000 per annum for 1 year.

## SECTION 4. PUBLICATIONS

### Journal Papers Arranged by Sub-topics:

#### Phase Transformations

- "Phase Stability of Chemically Derived Enstatite ( $\text{MgSiO}_3$ ) Powders," C. M. Huang, D. H. Kuo, Y. J. Kim and W. M. Kriven, J. Am. Ceram. Soc., 77 [10] 2625-2631 (1994).
- "High Temperature Phase Transformation in  $\text{Y}_4\text{Al}_2\text{O}_9$ ,  $\text{Gd}_4\text{Al}_2\text{O}_9$  and  $\text{Dy}_4\text{Al}_2\text{O}_9$ ," W. M. Kriven, J. L. Shull, W. D. Porter and C. A. Hubbard. In Solid  $\rightarrow$  Solid Phase Transformations in Inorganic Materials '94, (1994), 95-100.
- "Twinning in Structural Ceramics," W. M. Kriven. (invited review paper) in Twinning in Advanced Materials, Edited by M. H. Yoo and M. Wuttig. Published by The Minerals, Metals and Materials Society (TMS), Warrendale, PA., 435-448 (1994).
- "A Transmission Electron Microscopy Study on the Decomposition of Synthetic Hillebrandite ( $\text{Ca}_2\text{SiO}_4 \cdot \text{H}_2\text{O}$ )," Y. J. Kim and W. M. Kriven, J. Materials Research, 10 [12] 3084 - 3095 (1995). (From AFOSR URI 90-0174).
- "Displacive Phase Transformations and Their Applications in Structural Ceramics," W. M. Kriven, J. de Physique IV, Colloque C8 (1995), pp 101-110.
- "On the Role of Deformation Twinning in Domain Reorganization and Reorientation in Ferroelastic Crystals," P. Mullner and W. M. Kriven, J. Mater. Res., accepted (1996).
- "Phase Transformation in  $\text{KNbO}_3$  Perovskite Ceramic," O. O. Popoola and W. M. Kriven, Philosophical Magazine Letters, (1996) in press. (From AFOSR URI 90-0174)
- "Crystallography and Microstructural Studies of Phase Transformations in Dysprosia ( $\text{Dy}_2\text{O}_3$ )," Y. J. Kim and W. M. Kriven, Philosophical Magazine, submitted. (From AFOSR URI 90-0174).
- "Shear Induced Transformation in Enstatite," D. Zhu and W. M. Kriven, Cer. Sci. and Eng. Proc. 17A (1996) 383-390.

TRANSFORMATION WEAKENED INTERPHASES, S.J. Lee and W.M. Kriven,  
Department of Material Sciences and Engineering, University of Illinois at Urbana-  
Champaign, Urbana, IL. 61801

Laminates of  $\beta$ -cristobalite and mullite/cordierite mixtures in 60:40 wt% respectively were tape cast. The chemically stabilized  $\beta$ -cristobalite form with  $\text{Ca}^{2+}$ ,  $\text{Al}^{3+}$  stuffing cations was prepared by the Pechini process. The critical grain size of  $\beta$ -cristobalite for weakening transformation and fracture behavior were investigated at different thickness ratio of densified laminates by hot-pressing. The grain size was controlled by annealing process at 1300 °C. A load-deflection curve of 6h annealed sample showed a significant work of fracture ( $1.12 \text{ kJ/m}^2$ ) with a strength of 131 MPa at the thickness ratio between mullite/cordierite and  $\beta$ -cristobalite of 6:1. A low strength in spite of increasing work of fracture above a critical grain size of  $3 \mu\text{m}$  was attributed to the crack deflection by microcracks in the cristobalite layer. A severe microcrack occurred by thermally induced phase transformation, which is a cause of decreasing strength and work of fracture at long time annealing.

- "Shear Induced Transformation and Plasticity in Enstatite," D. Zhu and W. M. Kriven, *Acta. Metall. et Mater.*, submitted.

### Coatings

- "Laser Ablated Coatings on Ceramic Fibers for Ceramic Matrix Composites," C. M. Huang, F. Xiong, Y. Xu, A. Zangvil and W. M. Kriven, *J. Materials Science and Engineering*, **A191** (1995) 249-256.
- "Microstructure of Nanocrystalline NbAl<sub>3</sub>/Al Microlaminated Multilayer Thin Films Deposited by Pulsed Eximer Laser Ablation," H. Chung, M. J. Jilavi, T. P Duffey, J. Mazumder and W. M. Kriven, *Acta Met. et Mater.*, submitted.

### Monazite (LaPO<sub>4</sub>) and Zenotime (YPO<sub>4</sub>) Interfaces

- "Chemical Stability, Microstructure and Mechanical Behavior of LaPO<sub>4</sub>-Containing Ceramics," D. H. Kuo and W. M. Kriven, *J. Materials Science and Engineering* **A210** [1-2] (1996) 123-134.
- "Characterization of Yttrium Phosphate and a Yttrium Phosphate/Yttrium Aluminate Laminate," D. H. Kuo and W. M. Kriven, *J. Amer. Ceram. Soc., Comm.* **78** [11] 3121-3124 (1995).
- "Control of Interfacial Properties Through Fiber Coatings: Monazite Coatings in Oxide/Oxide Composites," D. H. Kuo, W. M. Kriven and T. J. Mackin, *J. Am. Ceram. Soc.*, (1997) in press.
- "Microstructure and Mechanical Response of Lanthanum Phosphate/Yttrium Aluminate and Yttrium Phosphate/Yttrium Aluminate Systems," D. H. Kuo and W. M. Kriven, *Cer. Sci. and Eng. Proc.* **17B** (1996) 233-240.
- "Development of Yttrium Phosphate as an Oxide/Oxide Interphase Material," D. H. Kuo and W. M. Kriven, *Proc. 2nd Int. Meeting of Pacific Rim Ceramic Societies (PACRIM 2)*, Cairns, Australia, July 15-17, (1996), accepted.
- "Interface Properties of YPO<sub>4</sub>/Y<sub>3</sub>Al<sub>5</sub>O<sub>12</sub> Systems: A Double Sandwich System and a Fiber Model Composite," D. H. Kuo and W. M. Kriven, *Ceramic Transactions* **74** (1996) 71-82.
- "A Strong and Damage-Tolerant Oxide Laminate," D. H. Kuo and W. M. Kriven, *J. Am. Ceram. Soc.* (1996) accepted.
- "Oxide Laminates with High Strength and Work of Fracture," D. H. Kuo and W. M. Kriven, Mat. Res. Soc. Symp. on Interface Engineering for Optimized Properties, (1997), submitted.

### Mullite and Mullite Fibers

- "Elastic Properties of Mullite," H. Ledbetter, S. Kim, S.D. Crudele and W. M. Kriven, J. Am. Ceram. Soc., in press.
- "Synthesis and Microstructure of Mullite Fibers Grown From Deeply Undercooled Melts," W. M. Kriven, D. Zhu and M. H. Jilavi, K. R. Weber, B. Cho, J. Felten, and P. C. Nordine. Ceramic Microstructures '96, edited by A. P. Tomsia and A. M. Glaeser, Plenum Pub., (1996) in press.

### SiC Fiber/Carbon-coated Interface Mechanics in SiAlON and Cementitious Materials

- "Combustion Synthesized  $\beta'$ -SiAlON Composites Reinforced with SiC Monofilaments," C. M. Huang, Y. Xu, D. Zhu and W. M. Kriven, J. Materials Science and Engineering, **A188** (1994) 341-351.
- "Residual  $\alpha$ -Si<sub>3</sub>N<sub>4</sub> Inclusions in Ce-doped O'+ $\beta$ -SiAlON Composites," Y. Xu, C. M. Huang, W. M. Kriven and A. Zangvil, J. Am. Ceram Soc. Comm., **77** [8] (1994) 223-2216.
- "Processing and Microstructure Characterization of a Ce-Doped, In-Situ Fabricated O'+ $\beta$ -SiAlON Composite," W. M. Kriven, C. M. Huang, Y. Xu, A. Zangvil and D. N. Coon, Ceram. Sci. Eng. Proc., **15-B** (1994) [5] 1128-1137.
- "A SiC/Combustion-Synthesized  $\beta'$ -SiAlON Composite," C. M. Huang, Y. Xu, D. Zhu and W. M. Kriven. Cer. Sci. Eng. Proc., **15-B** (1994) [5] 1154-1163. Poster won 3rd Prize at the 18th Annual Cocoa Beach Conf. and Exposition on Composites and Advanced Ceramics, Jan 19-24th (1994).
- "Interfacial Properties of SiC Monofilament Reinforced  $\beta'$ -SiAlON Composites," C. M. Huang, D. Zhu, Y. Xu, T. Mackin and W. M. Kriven, J. Materials Science and Engineering, (1995) **A201** 159-168.
- "Interfacial Bonding and Friction in SiC Monofilament/ $\beta'$  SiAlON Composites," C. M. Huang, Y. Xu, D. Zhu, T. Machin and W. M. Kriven, Ceramic Transactions, **46** (1994) 815-826.
- "SiC<sub>f</sub>/O'-SiAlON Composite: Properties and Oxidation Retained Properties," C. M. Huang, D. Zhu, Y. Xu, W. M. Kriven and C. Y. Yuh, J. Materials Science and Engineering, **A220** [1-2].176-184 (1996)

- "MoSi<sub>2</sub>-β' SiAlON Particulate Ceramic Composite," C. M. Huang, C. Y. Yuh, M. Farooque, D. Zhu, Y. Xu and W. M. Kriven, Cer. Sci. and Eng. Proc. 17A (1996) 295-302.
- "Interfacial Bonding of Carbon-Coated, Glass Fiber Reinforced Cement," C. M. Huang, D. Zhu, C. X. Dong and W. M. Kriven, Cer. Sci. and Eng. Proc. 17B (1996) 258-265.
- "Carbon-Coated Glass Fiber Reinforced Cement Composites: I. Fiber Push-out and Interfacial Properties," C. M. Huang, D. Zhu, C. X. Dong, W. M. Kriven, R. Loh and J. Huang, J. Am. Ceram. Soc. (1996) submitted.
- "Tape Cast MoSi<sub>2</sub>/β'-SiAlON Composite Reinforced with SiC Monofilaments," C. M. Huang, W. T. Y. Ho, C. Y. Yuh and M. Farooque, D. Zhu and W. M. Kriven, Ceramic Transactions 74 (1996) 459-470.
- "Properties and Microstructure of MoSi<sub>2</sub> - β' SiAlON Particulate Ceramic Composites," C. M. Huang, C. Y. Yuh, M. Farooque, D. Zhu, Y. Xu and W. M. Kriven, J. Am. Ceram. Soc. (1996) submitted.
- "Interfacial Modification of Fiber Reinforced Cement Composites, C. M. Huang, C. Y. Yuh, D. Zhu and W. M. Kriven. Mat. Res. Soc. Symp. on Interface Engineering for Optimized Properties," (1997), submitted.

#### Journal Papers in Preparation:

- "Transformation Weakened Interfaces in Ceramic/Ceramic Composites," W. M. Kriven, C. M. Huang, D. Zhu, Y. Xu and S. M. Mirek, for J. Am. Ceram. Soc.
- "Mullite Laminates with Cristobalite Transformation Weakened Interphases," S. J. Lee and W. M. Kriven, for J. Am. Cer. Soc.
- "Phase Stability of MgSiO<sub>3</sub> in the Forms of Powder, Pellet and Composite," D. H. Kuo and W. M. Kriven. For J. Am. Ceram. Soc.
- "Laser Ablated Oxide Coatings for Oxide Fibers," M. H. Jilavi, H. Chung, J. Mazumder and W. M. Kriven. For Cer. Sci. and Eng. Proc., Jan 1997.
- "Electron Microscopy Characterization and Evaluation of Oxide Fibers," D. Zhu, M. Jilavi and W. M. Kriven. For Cer. Sci. and Eng. Proc.

- "A Novel Technique for Producing Ceramic Fibers," J. J. Felten, J. K. Weber, P. C. Nordine, B. Cho, N. Lockwood, W. M. Kriven, M. Jilavi, and D. Zhu. For Cer. Sci and Eng. Proc.
- "Fabrication, Microstructure and Mechanical Response of Zirconia Containing Lanthanum Phosphate and Yttrium Phosphate Laminates," D. H. Kuo and W. M. Kriven. For Cer. Sci. and Eng. Proc.

#### Conference Proceedings:

- "In Situ TEM Study of Hillebrandite ( $\text{Ca}_2\text{SiO}_4 \cdot \text{H}_2\text{O}$ ) Decomposition," Y. J. Kim and W. M. Kriven, Proc. 13th Int. Congr. on Electron Microscopy (ICEM 13), Paris. (1994) Vol 2A, 545-547. (From AFOSR URI 90-0174).
- "*In Situ* Fabricated Ce-Doped  $\text{O}' + \beta'$  SiAlON Composites," C. M. Huang, Y. Xu, A. Zangvil and W. M. Kriven. Proc. 5th Int. Symp. on Ceramic Materials And Components for Engines, Paper No. P3/5 May 29th-June 1st 1994. Shanghai, China.
- "In-situ TEM study of the Cubic to Tetragonal Phase Transformations in  $\text{KNbO}_3$ ," O. O. Popoola and W. M. Kriven. Proc. 13th Int. Congr. on Electron Microscopy (ICEM 13), (Paris. (1994) Vol 2A, 549-551). (From AFOSR URI 90-0174).
- "SiC Monofilament Reinforced  $\beta'$ - and  $\text{O}'$ -SiAlON Composites," C. M. Huang, Y. Xu, D. Zhu and W. M. Kriven. Proc Int. Conf. on Composites Engineering (ICCE/1), Ed. David Dui. 269-270 (1994).
- "High Strength SiC Monofilament-reinforced MDF Cement," W. M. Kriven\*, C. M. Huang, D. Zhu and P. G. Desai. In Proc. of First Int. Conf. on Composites Engineering (ICCE/1). Edited by D. Hui, New Orleans, (1994) 223-224 .



## SECTION 5. INTERACTIONS/TRANSITIONS

### (a) Participation at meetings, conferences, seminars

#### Invited lectures and seminars

- \*\* "Phase Transformations in Ceramics," W. M. Kriven\*. Invited talk, presented at the Microscopy Society of America (MSA) Annual Meeting, held in Cincinnati in Aug 1-6, (1993).
- \*\* "Twinning in Structural Ceramics," W. M. Kriven.\* Invited lecture presented at TMS Annual Meeting in Symposium on Twinning in Advanced Materials. Held in Pittsburgh, PA, Oct 17-21, 1993.
- \*\* "Volume Changes During Transformation in Ceramics," W. M. Kriven.\* Invited lecture presented at the ASM Annual Meeting in Symposium on Effect of Plastic Deformation on the Thermodynamics, Kinetics and Mechanisms of Phase Transformations". Held in Pittsburgh, PA, Oct 17-21, 1993.
- \*\* "Ceramics Via Organic and Inorganic Synthesis," W. M. Kriven\*. Invited lecture presented to the Illinois Association of Chemistry Teachers, Annual Meeting at the University of Illinois at Urbana-Champaign, March 4th (1994)
- \*\* "Displacive and Martensitic Transformations in Ceramics," W. M. Kriven.\* Invited keynote lecture presented at International Conference on Solid to Solid Phase Transformations in Inorganic Materials '94. Held in Pittsburgh in July 17-22, (1994)
- \*\* "Current Trends in Structural Ceramics," W. M. Kriven. Invited plenary lecture presented at the Austceram '94, International Ceramic Conference. Held in Sydney, Australia, July 25-27, (1994)
- \*\* "Current Trends in Structural Ceramics," W. M. Kriven. Invited lecture presented at the Pacific Coast Regional Meeting of the American Ceramic Society, Oct 19-22, (1994), Los Angeles.
- \*\* "TEM Studies of Calcium Silicate Hydrates," W. M. Kriven.\* Invited lecture presented at Festive Symposium in honor of Professor T. Mitsuda of the Nagoya Institute of Technology, Ceramics research Laboratory. Held in Nagoya, Japan, Feb 24th (1995)
- \*\* "Displacive Transformations and Their Applications in Structural Ceramics," W. M. Kriven,\* invited review paper presented at the Int. Conf. on Martensitic Transformations (ICOMAT 95), held in Lausanne, Switzerland, Aug 20-25th (1995).

- \*\* "Phase Transformations and Their Applications in Ceramics," W. M. Kriven,\* invited lecture at Symposium to honor Professor Jack Christian on his 70th birthday. Held at Oxford University, UK, March 29th (1996).
- \*\* "Electron Microscopy Characterization of Melt-Grown Mullites and Mullite Fibers," W. M. Kriven,\* R. A. Gronsky and J. A. Pask, M. H. Jilavi, D. Zhu, J. J. Felten, J. K. R. Weber and P. C. Nordine, (invited) paper presented at Int. Conf. on Ceramic Microstructures'96: Control at the Atomic Level," held June 24-27 (1996), in Berkeley, CA, USA.
- \*\* "Transformation Weakening of Ceramic Composite Interphases," W. M. Kriven,\* invited paper to be presented at a Nato sponsored conference on "Multilayered and Fiber-Reinforced Composites: Problems and Prospects," to be held in Kiev in May 1997.
- \*\* "Synthesis of Oxide Powders by a Stearic Complexation Precursor Route," W. M. Kriven\*, invited paper to be presented at The 4th International Union of Materials Research Societies (IUMRS) Conference in Asia Makuhari, Chiba, Japan, September 16-18, 1997.

#### Conference Presentations

- "Transformation Mechanisms and Induced Fracture in Ceramics," W. M. Kriven\*. Presented at the Materials Research Society, Spring Meeting, held in San Fransisco, California in April 16-18th 1993.
- "Transformation-Induced Fracture in Ceramic Composites," W. M. Kriven\*. Invited talk, presented at the Annual Meeting of the American Ceramic Society, held in Cincinnati in April 18-22, 1993.
- "Phase Transformations in Chemically Derived Enstatite Powders," D. H. Kuo\*, C. M. Huang, Y. J. Kim and W. M. Kriven. Presented at the Annual Meeting of the American Ceramic Society, held in Cincinnati in April 18-22nd, 1993.
- "TEM Study of Synthetic Hillebrandite ( $\text{Ca}_2\text{SiO}_4 \cdot \text{H}_2\text{O}$ ), Y. J. Kim,\* W. M. Kriven and T. Mitsuda. Presented at the Annual Meeting of the American Ceramic Society, held in Cincinnati in April 18-22nd, 1993.
- "Transformation Mechanisms in Distrontium Silicate ( $\text{Sr}_2\text{SiO}_4$ )," Y. J. Kim\*, J. L. Shull Jr., and W. M. Kriven. Presented at the Annual Meeting of the American Ceramic Society, held in Cincinnati in April 18-22nd, 1993.

- "The Orthorhombic (o) to Tetragonal (t) Transformation in  $\text{KNbO}_3$ ," O. O. Popoola\* and W. M. Kriven. Presented at the Annual Meeting of the American Ceramic Society, held in Cincinnati in April 18-22nd, 1993.
- "Processing and Mechanical Properties of Alumina Platelet Reinforced Zirconia," I. K. Cherian,\* I. Nettleship and W. M. Kriven. Presented at the Annual Meeting of the American Ceramic Society, held in Cincinnati in April 18-22, 1993.
- "Calcination Behavior of Chemically Prepared Calcium Aluminate," M. A. Gulgun\*, O. O. Popoola and W. M. Kriven. Presented at the Annual Meeting of the American Ceramic Society, held in Cincinnati in April 18-22nd, 1993.
- "Crystal Growth and Characterization of Distronium Silicate," B. N. Sun\*, J. L. Shull and W. M. Kriven. Presented at the Annual Meeting of the American Ceramic Society, held in Cincinnati in April 18-22nd, 1993.
- "Synthesis of Silicate and Aluminate Powders by a Modified Pechini Process," M. A. Gulgun\*, C. M. Huang, D. H. Kuo, J. L. Shull\*, K. G. Slavick, T. K. Swanson, W. M. Kriven, I. Nettleship and R. Russel. Presented at the Annual Meeting of the American Ceramic Society, held in Cincinnati in April 18-22nd, 1993.
- "TEM Investigation of Crystallization Kinetics in Calcium Aluminate Powders," M. A. Gulgun\*, O. O. Popoola and W. M. Kriven. Presented at the Joint Meeting of the Central States Electron Microscopy Society, Sangamon State University, Springfield, Illinois, May 20th 1993.
- "Phase Transformation Induced Intragranular Microcracks in Enstatite," D. H. Kuo\*, C. M. Huang, Y. J. Kim and W. M. Kriven. Presented at the Joint Meeting of the Central States Electron Microscopy Society, Sangamon State University, Springfield, Illinois, May 20th 1993.
- "Pretransitional Phenomena, Transformation Mechanisms and Crystallography of  $\text{PbTiO}_3$  and  $\text{KNbO}_3$ ," H. Chen\*, C. M. Wayman, W. M. Kriven and J. D. Bass. Presented at 8th International Meeting on Ferroelectricity (IMF8) held at NIST in August, 1993.
- "Processing and Microstructure Characterization of an In-Situ Fabricated  $\text{O}' + \beta\text{-SiAlON}$  Composite," C. M. Huang\*, Y. Xu, A. Zangvil, W. M. Kriven and D. N. Coon. Abstract #[CP-21-94F] presented at 18th Annual Cocoa Beach Conf. and Exposition on Composites and Advanced ceramics, Jan 9-14, 1994.

- "A SiC/Combustion-Synthesized  $\beta'$ SiAlON Composite," C. M. Huang\* Y. Xu, D. Zhu and W. M. Kriven, Abstract #[CP-26-94F] presented at 18th Annual Cocoa Beach Conf. and Exposition on Composites and Advanced ceramics, Jan 9-14, 1994. This poster won third prize in the Professional Section Poster competition.
- "Chemically Bonded Ceramics as an Alternative to High Temperature Composite Processing," B. R. Johnson, M. A. Gulgun\* and W. M. Kriven. Abstract #[N5.97] presented at the Spring Meeting of the Materials Research Society, San Francisco, April 4-8 1994.
- "TEM Study of the Decomposition of Synthetic Hillebrandite," Y. J. Kim and W. M. Kriven\*. Presented at the Annual Meeting of the American Ceramic Society, Indianapolis, IN, April 24-28 1994.
- "Interfacial Bonding and Friction in a SiC Monofilament/ $\beta'$  SiAlON Composite," C. M. Huang\*, Y. Xu, D. Zhu and W. M. Kriven. Presented at the Annual Meeting of the American Ceramic Society, Indianapolis, IN, April 24-28 1994.
- "Fabrication by Colloidal Filtration of Alumina Platelet Reinforced 3Y-TZP: Mechanical Properties," I. K. Cherian\* and W. M. Kriven. Presented at the Annual Meeting of the American Ceramic Society, Indianapolis, IN, April 24-28 1994.
- "Phase Transformations in Rare Earth Aluminates ( $2\text{Ln}_2\text{O}_3 \cdot \text{Al}_2\text{O}_3$ )," J. L. Shull\*, C. Beckman and W. M. Kriven. Presented at the Annual Meeting of the American Ceramic Society, Indianapolis, IN, April 24-28 1994.
- "Phase Transformations in Potassium Niobate Perovskite Ceramic," O. O. Popoola and W. M. Kriven\*. Presented at the International Conference on Solid to Solid Phase Transformations, Pittsburgh, PA July, 1994.
- "The Mechanism of the Tetragonal to Monoclinic Transformation in  $\text{YNbO}_4$ ," J. L. Shull\*, B. N. Sun and W. M. Kriven. Presented at the International Conference on Solid to Solid Phase Transformations, Pittsburgh, PA July, 1994.
- "High Temperature Phase Transformations in  $\text{Y}_4\text{Al}_2\text{O}_9$ ,  $\text{Gd}_4\text{Al}_2\text{O}_9$  and  $\text{Dy}_4\text{Al}_2\text{O}_9$ ," J. L. Shull\* and W. M. Kriven. Presented at the International Conference on Solid to Solid Phase Transformations, Pittsburgh, PA July, 1994.

- "SiC Monofilament Reinforced  $\beta'$ - and O'-SiAlON Composites," C. M. Huang\*, Y. Xu, D. Zhu and W. M. Kriven. Presented at First International conference on Composites Engineering, held in New Orleans, LA, Aug 28-31, 1994.
- "In Situ Fabricated O' +  $\beta'$  SiAlON Mixed Ceramic Composites," C. M. Huang\* and W. M. Kriven. Abstract # [B-64-94F] presented at the Fall Meeting of the American Ceramic Society, held in Louisville, Kentucky, Sept 25-28, 1994.
- "Chemically Bonded Ceramic Matrix Composites: Densification and Conversion to Diffusion Bonding," B. R. Johnson\*, M. A. Gulgun and W. M. Kriven. MRS Fall Meeting, Boston Dec 1994.
- "Interfacial Properties of SiC Fiber Reinforced MDF Composite," D. Zhu\*, C. M. Huang and W. M. Kriven. Abstract [# T-11-95] presented at the Annual Meeting of the American Ceramic Society, Cincinnati, Ohio, April 30 - May 3rd (1995).
- "Ferroelasticity in  $\text{Ca}_2\text{SiO}_4$ ,  $\text{Sr}_2\text{SiO}_4$  and  $\text{Ba}_2\text{SiO}_4$ ," J. L. Shull\* and W. M. Kriven. Abstract [#BP-09-95] presented at the Annual Meeting of the American Ceramic Society, Cincinnati, Ohio, April 30 - May 3rd (1995).
- "A Simple Solution-Polymerization Route for Oxide Powders," M. A. Gulgun\* and W. M. Kriven. Abstract [# SXIXP-2-95] presented at the Annual Meeting of the American Ceramic Society, Cincinnati, Ohio, April 30 - May 3rd (1995).
- "Chemically Bonded Ceramic Processing of Monocalcium Aluminate," B. R. Johnson, M. A. Gulgun and W. M. Kriven\*. Abstract [# SXIX-73-95] presented at the Annual Meeting of the American Ceramic Society, Cincinnati, Ohio, April 30 - May 3rd (1995).
- "Transformation Weakening of Ceramic Composite Interfaces," W. M. Kriven\*, C. M. Huang, D. Zhu, Y. Xu, and S. C. Mirek. Abstract # [C-115-96F]. Presented at 20th Annual Cocoa Beach Conf. and Exposition on Composites and Advanced Ceramics, Jan 7-11th (1996).
- "Behavior of Shear Induced Constrictive Transformation in Enstatite, D. Zhu\* and W. M. Kriven. Abstract #[C-99-96F]. Presented at 20th Annual Cocoa Beach Conf. and Exposition on Composites and Advanced Ceramics, Jan 7-11th (1996).

- "Fabrication, Microstructure and Mechanical Response of Lanthanum Phosphate/ Yttrium Aluminate and Yttrium Phosphate/Yttrium Aluminate Systems," D. H. Kuo\* and W. M. Kriven. Abstract #[C-118-96F]. Presented at 20th Annual Cocoa Beach Conf. and Exposition on Composites and Advanced Ceramics, Jan 7-11th (1996).
- "Interfacial Bonding of Carbon-Coated Glass Fiber Reinforced Cement," C. M. Huang\*, R. Loh, J. Huang, D. Zhu and W. M. Kriven. Abstract "[CP-12-96F]. Presented at 20th Annual Cocoa Beach Conf. and Exposition on Composites and Advanced Ceramics, Jan 7-11th (1996).
- " $\beta$ -SiAlON/MoSi<sub>2</sub> Particulate Ceramic Composite," C. M. Huang\*, C. Y. Yuh, M. Faroque, D. Zhu and W. M. Kriven. Abstract # [CP-14-96F]. Presented at 20th Annual Cocoa Beach Conf. and Exposition on Composites and Advanced Ceramics, Jan 7-11th (1996). Won second prize in the Poster Competition.
- "Interfacial Properties of a YAG Fiber/Ceramic Matrix Composite with an YPO<sub>4</sub> Interphase," D. H. Kuo\*, W. M. Kriven and T. J. Mackin. Presented at 98th Annual Meeting of the American Ceramic Society, Indiannapolis, IN April 14-17th (1996).
- "Transformation Weakening of Interphases in Oxide Composites," W. M. Kriven\*, C. M. Huang, D. Zhu, Y. Xu and S. C. Mirek. Presented at 98th Annual Meeting of the American Ceramic Society, Indiannapolis, IN April 14-17 (1996).
- "The Effect of LaPO<sub>4</sub> Coating Thickness on Interfacial Mechanics of YAG and Al<sub>2</sub>O<sub>3</sub> Fiber Reinforced Alumina Matrix Composites, D. H. Kuo, W. M. Kriven and T. J. Mackin\*. Presented at 98th Annual Meeting of the American Ceramic Society, Indiannapolis, IN April 14-17th (1996).
- "Electron Microscopy Characterization of Melt-Grow Mullites and Mullite Fibers," W. M. Kriven\*, R. A. Gronsky and J. A. Pask, M. H. Jilavi, D. Zhu, J. J. Felten, J. K. R. Weber and P. C. Nordine, (invited). Paper presented at Int. Conf. on Ceramic Microstructures'96: Control at the Atomic Level," held June 24-27 (1996), in Berkeley, CA, USA.
- "Transformation Weakening of Oxide Interphases and Comparison with other Debonding Mechanisms," W. M. Kriven\*, C. M. Huang, D. Zhu, Y. Xu and S. C. Mirek. Presented at the 2nd Int. Meeting of Pacific Rim Ceramic Societies (PACRIM 2), held in Cairns, Australia, July 15-17, (1996).

- "Development of Yttrium Phosphate as an Interphase for Oxide/Oxide Composites," D. H. Kuo and W. M. Kriven,\* Presented at the 2nd Int. Meeting of Pacific Rim Ceramic Societies (PACRIM 2), held in Cairns, Australia, July 15-17, (1996).
- "Interfacial Modification of Fiber Reinforced Cement Composites, C. M. Huang,\* C. Y. Yuh, D. Zhu and W. M. Kriven. [Abstract #HH8.3] presented at the Materials Research Society Fall Annual Meeting, Boston MA, Dec 2-6 (1996).
- "Oxide Laminates with High Strength and Work of Fracture," D. H. Kuo\* and W. M. Kriven, Invited paper [abstract # W12.6] presented at the Materials Research Society Fall Annual Meeting, Boston MA, Dec 2-6 (1996).
- "Electron Microscopy Characterization and Evaluation of Oxide Fibers," D. Zhu, M. H. Jilavi and W. M. Kriven,\* to be presented at the 21st Annual Cocoa Beach Conference and Exposition Jan 12-16th (1997), Cocoa Beach, Florida.
- "Laser Ablated Oxide Coatings for Oxide Fibers, M. H. Jilavi, W. M. Kriven,\* H. Chung, and J. Mazumder, to be presented at the 21st Annual Cocoa Beach Conference and Exposition Jan 12-16th (1997), Cocoa Beach, Florida.
- "A Novel Technique for Producing Ceramic Fibers," J. J. Felten\*, J. K. R. Weber, P. C. Nordine, B. Cho, N. Lockwood, W. M. Kriven, M. H. Jilavi, and D. Zhu. To be presented at the 21st Annual Cocoa Beach Conference and Exposition Jan 12-16th (1997), Cocoa Beach, Florida.
- "Fabrication, Microstructure and Mechanical Response of Zirconia Containing Lanthanum Phosphate and Yttrium Phosphate Laminates," D. H. Kuo\* and W. M. Kriven, To be presented at the 21st Annual Cocoa Beach Conference and Exposition Jan 12-16th (1997), Cocoa Beach, Florida.

**(b) Consultative and advisory functions**

Consulting for United Technologies Corp., Pratt and Whitney Operations Branch, Florida, on high temperature oxide materials for aerospace applications.

**(c) Transitions**

- A Small Business Innovative Research (SBIR) was awarded jointly with Containerless Research Inc., for the fabrication of mullite and YAG fibers. Stage I was in operation from Sept 1995 to Feb 1996. Stage II was not awarded.
- A Science and Technology Transfer (STTR) contract with the Containerless Research Inc., Evanston, IL, was awarded for directional crystallization of oxide (e.g., mullite and YAG) fibers. Contract is through the AFOSR and is due to start on Oct 1st 1996 for six months.

**(d) Interdisciplinary Collaborations**

- Have co-authored on publication on applying the PELA laser ablation technique to coat ceramic fibers with ceramics, with Dr. F. Xiong of the BIRL at Northwestern University, Evanston, IL.
- Have co-authored two publications in the area of deposition of coatings by PELA with Professor Jyoti Mazumder, Director of the Center for Laser Aided Fabrication, in the Dept. of Mechanical and Industrial Engineering, UIUC.
- Have co-authored two publications with Professor Thomas Mackin, Assistant Professor, Dept. of Mechanical and Industrial Engineering, UIUC.
- Collaboration is in progress in the measurement of debonding behavior of fluorophlogopites by fiber pushout testing. The system was devised by Professor Bill Petuskey of the Dept of Chemistry and Biochemistry at Arizona State University, Tempe, AZ. The coating powders were supplied by Professor Petuskey and the composite is being fabricated and evaluated at UIUC.



## SECTION 6. NEW DISCOVERIES, PATENTS OR PATENT DISCLOSURES

- "Toughening of Ceramics by Transformation Weakening of Interphases," by W. M. Kriven, C. M. Huang, D. Zhu, Y. Xu and S. C. Mirek. Disclosure filed on Aug 14th 1996. A reduction to practise disclosure is in preparation.
- "A High-Strength, High Toughness Oxide Ceramic Composite," by D. H. Kuo and W. M. Kriven. Disclosure filed on June 5th 1996. Patent is currently being filed.

## SECTION 7. HONORS OR AWARDS

### Received during Grant period:

- Professor Kriven was promoted to Full Professor in Sept 1995.
- Professor Kriven was made a Fellow of the American Ceramic Society in April (1995).
- Professor Kriven received several prestigious invitations to give plenary and keynote lectures at international conferences and meetings as described in previous sections.
- Best Poster Award, Third Prize, from the Engineering Ceramic Division of the American Ceramic Society. For poster presented at the 18th Annual Conference on Composites and Advanced Ceramics, Jan 9-14th (1994).
- Best Poster Award, Second Prize, from the Engineering Ceramic Division of the American Ceramic Society. For Poster presented at the 19th Annual Conference on Composites and Advanced Ceramics, Jan 7-11th (1996).

### Received prior to Grant period

- Brunauer Award (1988), jointly with Dr. C.J. Chan. and Prof. J.F. Young. Awarded by the Cements Division of the American Ceramic Society, for the Best Paper of the Year.
- Brunauer Award (1991), jointly with Dr. O.O. Popoola and Prof. J.F. Young. Awarded by the Cements Division of the American Ceramic Society, for the Best Paper of the Year.

**SECTION 8****SYNOPSIS OF THESIS**

Copies of theses may be obtained from:  
The Grainger Engineering Library Reference Center  
University of Illinois at Urbana-Champaign  
1301 West Springfield Ave.,  
Urbana IL 61801  
Tel: (217) 244 7826  
Fax: (217) 244 7764

PHASE TRANSFORMATION WEAKENING IN  
FIBROUS CERAMIC COMPOSITES; AN INVESTIGATION OF  
THE ENSTATITE ( $\text{MgSiO}_3$ )/TITANIA ( $\text{TiO}_2$ ) SYSTEM

BY

STEVEN CHAD MIREK

B.S., Bradley University, 1993

THESIS

Submitted in partial fulfillment of the requirements  
for the degree of Master of Science in Materials Science and Engineering  
in the Graduate College of the University of  
Illinois at Urbana - Champaign, 1995

Urbana, Illinois

## TABLE OF CONTENTS

CHAPTER 1: INTRODUCTION.....	1
1.1 Phase Transformation Weakening in Ceramic Composites...	1
1.2 Time for Something New.....	3
1.3 Research Objectives.....	6
CHAPTER 2: LITERATURE REVIEW.....	8
2.1 Transformation Weakening.....	8
2.1.1 Concepts and Theory.....	8
2.1.2 Applications to Structural Ceramics.....	11
2.2 Phase Transformation Theory.....	13
2.2.1 Classifications.....	13
2.2.2 Kinetics and Thermodynamics.....	15
2.2.3 Fracture Toughness Behavior.....	17
2.3 Polymorphs and Crystallography of $\text{MgSiO}_3$ .....	20
2.4 $\text{MgSiO}_3$ - $\text{TiO}_2$ Phase Equilibria.....	23
2.5 "Fibrous Monolithic Ceramics".....	24
2.5.1 A History.....	24
2.5.2 Fabrication.....	26
2.5.3 Microstructural Development and Characterization..	27
2.5.4 Mechanical Behavior.....	27
CHAPTER 3: EXPERIMENTAL PROCEDURE.....	29
3.1 Raw Materials.....	29
3.2 Powder Processing Via a Modified Pechini Process.....	29
3.3 Polymer Precursor Synthesis of $\text{MgSiO}_3$ .....	31

4.4.1 Sample Fabrication.....	66
4.4.2 Interfacial Properties.....	67
4.4.3 TEM Examination of the $\text{MgSiO}_3$ Interphase.....	72
4.5 Fibrous Ceramic Composites.....	78
4.5.1 Sample Fabrication.....	78
4.5.2 Mechanical Behavior and Microstructural Characterizations.....	80
4.5.3 Potential for Shear Stress Weakening of $\text{MgSiO}_3$ Interphases.....	90
CHAPTER 5: CONCLUSIONS.....	91
REFERENCES.....	93
APPENDIX 1: Raw Materials and Processing Aids.....	100
APPENDIX 2: Ultrasonic Testing Results for $\text{MgSiO}_3$ .....	104

## LIST OF FIGURES

<b>Figure 1.</b> The polymorphism of $\text{MgSiO}_3$ <sup>7</sup> .....	23
<b>Figure 2.</b> Phase diagram for the $\text{MgSiO}_3$ - $\text{TiO}_2$ binary system. Below a temperature of 1400 °C, $\text{MgSiO}_3$ and $\text{TiO}_2$ do not react to form intermediate compounds <sup>49</sup> .....	24
<b>Figure 3.</b> Flow chart illustrating the modified Pechini process <sup>55</sup> .....	30
<b>Figure 4.</b> Flow chart illustrating the fabrication of the model composite system.....	36
<b>Figure 5.</b> Schematic illustrations of the model system. (a) Top view. (b) Cross section.....	37
<b>Figure 6.</b> Hot isostatic press schedule developed for densification of the model composite system.....	38
<b>Figure 7.</b> Kinematic viscosity profiles for aqueous solutions of MPEG 550 <sup>TM</sup> .....	40
<b>Figure 8.</b> Typical rheology curves for DuPont's Elvax 470 <sup>TM</sup> . (a) Shear stress vs. shear rate. (b) Apparent melt viscosity vs. shear rate.....	41
<b>Figure 9.</b> Photograph of (a) granule pressing cylinder, (b) extrusion cylinder, (c) extrusion block, and (d) spinnerette as supplied in standard form from Bradford University Research Limited.....	43
<b>Figure 10.</b> Extrusion of fibrous ceramics. (a) After the first pass. (b) After the second pass.....	45
<b>Figure 11.</b> Flow chart illustrating the processing of fibrous ceramic composites.....	46
<b>Figure 12.</b> Burnout schedule developed to remove the Elvax 470 <sup>TM</sup> binder from the green billet.....	47

- Figure 23.** SEM micrograph of an average  $\text{TiO}_2$  particle after attrition.....65
- Figure 24.** SEM micrograph of average  $\text{MgSiO}_3$  crystallites after attrition.....66
- Figure 25.** Optical micrograph of the as-HIPed,  $\text{TiO}_2/\text{MgSiO}_3/\text{TiO}_2$ , model composite in cross section showing the uniform and fully-dense,  $\text{MgSiO}_3$ , interphase region.....67
- Figure 26.** Interfacial shear stress vs. displacement curve generated from pushout analysis for the as-HIPed and HIPed, then-annealed, model composites.....68
- Figure 27.** SEM micrograph of the as-HIPed model composite after pushout. Courtesy of Mehmet Gulgun.....69
- Figure 28.** SEM micrograph of the HIPed, then-annealed, model composite after pushout. Courtesy of Mehmet Gulgun.....70
- Figure 29.** SEM micrograph of the residual  $\text{MgSiO}_3$  layer on the pushed-out,  $\text{TiO}_2$ , cylinder surface in the HIPed, then-annealed, model composite. Courtesy of Mehmet Gulgun.....71
- Figure 30.** EDS spectrum identifying the residual layer on the pushed-out,  $\text{TiO}_2$ , cylinder surface of the HIPed, then-annealed, model composite to be  $\text{MgSiO}_3$ . Courtesy of Mehmet Gulgun.....71
- Figure 31.** TEM micrograph of the as-HIPed model composite illustrating the microstructure of the  $\text{MgSiO}_3$  interphase. Courtesy of Dr. Y. Xu.....72
- Figure 32.** Selected-area diffraction patterns in the as-HIPed model composite revealing the  $\text{MgSiO}_3$  interphase to be protoenstatite (PE). (a)  $[001]$  direction, (b)  $[1\bar{1}\bar{2}]$  direction, (c)  $[1\bar{1}3]$  direction. Courtesy of Dr. Y. Xu.....73
- Figure 33.** TEM micrograph of a faulted and/or twinned PE grain in the as-HIPed model composite. Courtesy of Dr. Y. Xu.....74



**Figure 44.** SEM micrograph illustrating  $\text{TiO}_2$  pullout in the hot-pressed, then-annealed, fibrous ceramic ( $1350^\circ\text{C}$  for 25 h).....89

**Figure 45.** XRD spectrum for  $\text{MgSiO}_3$  annealed at  $1300^\circ\text{C}$  for 15 h. Results indicate no CE development. Pattern collected at room temperature.....106

**Figure 46.** XRD spectrum for  $\text{MgSiO}_3$  hot pressed at  $1200^\circ\text{C}$  for 2 h at 34 MPa. Pattern collected at room temperature.....107

because both of these coatings are unsuitable for extended use at elevated temperatures in oxidizing environments. Clearly, a need exists for a new type of ceramic coating to be incorporated at the fiber/matrix interface so as to allow further development of brittle-matrix composites for high-temperature applications.

A new concept of phase transformation weakening at the interface of ceramic/ceramic composites has been investigated in this research.<sup>2</sup> First suggested by Bloor<sup>6</sup> in 1964, the concept of phase transformation weakening has led to the search for a displacive or martensitic phase transformation with a negative volume change accompanied with a large, unit-cell, angular, shape change.<sup>7</sup> Ideal material candidates would be incorporated at the reinforcement/matrix interface. While several materials are considered to be promising candidates, enstatite ( $\text{MgSiO}_3$ ) with its 5.5% volume shrinkage and 18.3° unit-cell shape change upon transformation from protoenstatite (PE) to clinoenstatite (CE) is the primary interest of this work.<sup>7</sup>

Salient features of this concept include:

- A negative volume change and angular shape change upon transformation in order to induce the weakening of the interface.
- The weakening effect being tailored by choice of transformation weakening material and its thickness.
- The potential to transform martensitically under the stress field associated with a propagating crack.
- Crack-tip, stress-induced phase transformation being responsible for fiber pullout, crack bridging, grain deflection, and frictional work associated with the crack as it moves along the fiber/matrix interface.

tailored "wood-like" architecture.<sup>4,9,10</sup> These advanced composites are ideal candidates for many high-temperature, oxidation-resistant, lightweight, structural components such as are found in gas turbine engines. Their main advantages include a non-linear, stress-strain relationship, high failure strain in tension, and outstanding resistance to crack propagation.

However, these materials have been used to a limited degree because of the high costs associated with their processing and fabrication. Fiber-reinforced ceramic-matrix composites contain expensive fibers and, in many cases, must be formed using costly processing techniques. Pulsed eximer laser ablation (PELA)<sup>11</sup> and chemical vapor deposition are two such techniques used in applying coatings to fibers. Chemical vapor infiltration is another costly processing method employed in the matrix formation of some composite systems. There would seem to exist a need for structural ceramic materials formed from inexpensive processing routes which show non-catastrophic fracture behavior.<sup>10</sup>

Traditional monolithic ceramic materials are brittle. Therefore, they exhibit poor fracture behavior and fail in a catastrophic manner. However, ceramics with duplex compositions have been shown to be flaw insensitive with R-curve behavior.<sup>9</sup> By tailoring microstructural designs, significant improvements in mechanical properties of these so-called "fibrous monolithic ceramics" can be obtained. Fibrous ceramics can be designed to interact with cracks and retard their propagation in order to improve fracture behavior.<sup>10</sup>

Clegg et al.<sup>5</sup> have demonstrated these concepts in SiC/graphite tape-cast laminates in which the graphite interlayers delaminated during failure and exhibited comparable flexural stress-strain behavior to that of fiber-reinforced

### 1.3 Research Objectives

The research is divided into two main parts with the overall goal of demonstrating, examining, and understanding the phenomenon of phase transformation weakening in a fibrous-ceramic system. This work is part of ongoing research collocating displacive phase transformations in structural ceramics. To date, little attention has been given to incorporating transformation weakeners at the interface in ceramic composites. It is hoped that a better understanding of phase transformation weakening as a potential toughening mechanism in the otherwise brittle ceramics will lead to further investigations and developments for high-temperature applications.

The first part of the research pertains to the development of a model system used to test the feasibility of the PE to CE transformation in a thermodynamically compatible system. It is of interest to fabricate composite archetypes from  $\text{MgSiO}_3$ -coated,  $\text{TiO}_2$  cylinders embedded in a  $\text{TiO}_2$  matrix so as to conduct cylinder-pushout testing in order to study weakening effects on interfacial properties of fabricated and fabricated, then-annealed samples. The appropriate characterization methods of transmission electron microscopy (TEM), scanning electron microscopy (SEM), optical microscopy (OM), energy dispersive spectroscopy (EDS), and x-ray diffraction (XRD) are used in the investigation of the model system.

The second part of the research focuses on the thermal inducibility of the PE to CE transformation in a fibrous ceramic. It is of scientific and engineering interest to study the effects of phase transformation weakening in a tailored design. An adapted version of the so-called "fibrous monolithic ceramic" approach employed by Halloran et al.<sup>10</sup> is used to fabricate dense,

## CHAPTER 5: CONCLUSIONS

Single-phase  $\text{MgSiO}_3$  (OE) powder has been prepared via a modified Pechini process and verified by XRD, SEM, and EDS. This polymerization method has allowed for a low-temperature synthesis of high-purity stoichiometric powders which make it superior to pre-existing, high-temperature, synthesis reactions involving  $\text{MgO}$  and  $\text{SiO}_2$ . Other important advantages associated with this process include homogeneous particle morphologies, small particle sizes, and relatively low costs as compared to other solution methods.

A model  $\text{TiO}_2/\text{MgSiO}_3/\text{TiO}_2$  composite has been fabricated using conventional forming techniques in order to study the feasibility of phase transformation weakening and interfacial properties in a thermodynamically compatible ceramic system. Pushout data has indicated significant weakening of the bonding at the matrix/cylinder interface and a decrease of 57% in the required shear stress for cylinder pushout. Electron microscopy has revealed the origin of the interfacial debonding to be within the  $\text{MgSiO}_3$  interphase indicating that the thermally-induced, PE to CE, phase transformation is the primary mechanism behind the investigated phenomenon.

A novel processing route has been used to develop a tailored microstructure in order to investigate the mechanical properties associated with phase transformation weakening in a fibrous ceramic. In contrast to the as-hot-pressed sample, the hot-pressed, then-annealed specimens have been shown to exhibit graceful or non-catastrophic failure after the first fracture event. Annealed for 10 h at 1350 °C, a fibrous ceramic composite retains

INVESTIGATION OF OXIDE FIBER/OXIDE MATRIX COMPOSITES  
WITH A WEAK INTERPHASE

BY

DONG-HAU KUO

B.S., Feng Chia University, 1985

M.S., National Cheng Kung University, 1987

THESIS

Submitted in partial fulfillment of the requirements  
for the degree of Doctor of Philosophy in Materials Science and Engineering  
in the Graduate College of the  
University of Illinois at Urbana-Champaign, 1996

Urbana, Illinois

## ABSTRACT

While non-oxide fiber-reinforced ceramic composites are important in structural composite applications, high temperature oxidation degrades their mechanical properties and limited their applications in advanced turbine engines and heat exchangers. A potential solution is to develop all-oxide fiber-reinforced composites. However, two major problems limiting progress are the absence of commercialized strong and creep resistant fibers and the need for interfacial debonding to allow energy dissipation and toughening mechanisms to operate.

The focus of this thesis is the modification of oxide fiber/oxide matrix interfacial bonding. To this end, the two model configurations studied were the coated fiber system and multilayered oxide laminates. Monazite ( $\text{LaPO}_4$ ) and zirconium (YPO<sub>4</sub>) were the candidate interphase materials.

The plan of this thesis is as follows. After an introductory chapter, there is a literature review discussing the existing toughening mechanisms for ceramics, the basic mechanics of fiber-reinforced ceramic composites, interface mechanics, and interface mechanical testing. We also review previous studies related to oxide fiber/oxide matrix composites, residual stress calculations of a three-cylinder model system, and strong and tough ceramics without reinforcements. We make four proposals in chapter 3. These proposals are related to the key contributions from this thesis.

Experimental procedures are then examined in detail in chapter 4. These procedures include the preparation of powders, laminates, and fiber model composites, and the mechanical evaluation by macromechanical (flexural testing) and micromechanical (fiber pushout testing) tests. Laminates were fabricated by a tape-casting technique followed by hot

pressing. Fiber model systems were fabricated by dip coating followed by sintering. Both laminates and fiber model composites can facilitate interface studies in an economic way. Three kinds of laminates were studied: simple laminate systems, laminates with different configurations, and  $\text{YPO}_4$ - and  $\text{LaPO}_4$ -containing  $\text{ZrO}_2$  laminates. Four kinds of fiber model composites were studied: a  $\text{LaPO}_4$ -coated single crystal sapphire ( $\text{Al}_2\text{O}_3$ ) fiber/ $\text{Al}_2\text{O}_3$  matrix composite; a  $\text{LaPO}_4$ -coated single crystal yttrium aluminum garnet (YAG) fiber/ $\text{Al}_2\text{O}_3$  matrix composite; a  $\text{LaPO}_4$ -coated YAG fiber/yttrium aluminate ( $\text{Y}_3\text{Al}_5\text{O}_{12}$ ) matrix composite; and a  $\text{YPO}_4$ -coated YAG fiber/ $\text{Y}_3\text{Al}_5\text{O}_{12}$  matrix composite. The first two fiber model composites can be described as  $\text{Al}_2\text{O}_3$ -matrix model composites, while the last two as  $\text{Y}_3\text{Al}_5\text{O}_{12}$ -matrix model composites.

Chapter 5 gives a thorough description of experimental results. In the study of chemical compatibility, the following systems were studied:  $\text{LaPO}_4/\text{Al}_2\text{O}_3$ ;  $\text{LaPO}_4/\text{Y}_3\text{Al}_5\text{O}_{12}$ ;  $\text{LaPO}_4/\text{lanthanum aluminate}$  ( $\text{LaAl}_{11}\text{O}_{18}$ );  $\text{LaPO}_4/\text{yttria-stabilized zirconia}$  ( $\text{Y-ZrO}_2$ );  $\text{YPO}_4/\text{Y}_3\text{Al}_5\text{O}_{12}$ ; and  $\text{YPO}_4/\text{Y-ZrO}_2$ . The coefficients of thermal expansion of  $\text{YPO}_4$  and  $\text{LaAl}_{11}\text{O}_{18}$  were measured. Flexural tests were executed on different kinds of laminates. Strength, toughness, and the weakness of interface bonding of these laminates were determined. A strong and tough oxide was identified in the  $\text{YPO}_4/\text{Y-ZrO}_2/30 \text{ vol\% Y-ZrO}_2\text{-}70 \text{ vol\% Al}_2\text{O}_3$  (YZ3-A7)/ $\text{Y-ZrO}_2$  laminate with a four-layered configuration. This laminate had four-point bend strengths of 358 and 392 MPa and apparent work-of-fracture values of 8.2 and 10  $\text{kJ/m}^2$ , respectively.

The results of interface mechanical tests are also described in chapter 5. Interface properties of four kinds of fiber model systems were obtained by analyzing pushout data with the linear model, the shear-lag model, and the Liang-Hutchinson model. These interface properties include interface fracture energy, coefficient of friction, clamping pressure, interface debond strength, and interface friction strength. A systematic study of the effect of



interphase coating thickness on interface properties and pushout response was performed on two  $\text{Al}_2\text{O}_3$ -matrix fiber model composites. A new test methodology was proposed in which a double-shear  $\Gamma_{II}$  test utilized a force-based, double-shear test and an energy-based fracture mechanics concept was applied to measure the interface properties of the  $\text{YPO}_4/\text{Y}_3\text{Al}_5\text{O}_{12}$  system.

Chapter 6 is the discussion section. Chemical reactions between  $\text{LaPO}_4$  and  $\text{Al}_2\text{O}_3$  and between  $\text{YPO}_4$  and  $\text{Al}_2\text{O}_3$  were explained. The importance of the thermal expansion effect on laminate fabrication was emphasized. Mechanical responses of the simple laminate systems and laminates with different configurations were discussed. It was noted that limited interface delamination of laminates was not enough to prevent laminates from catastrophic fracture. A strong and damage-tolerant  $\text{YPO}_4/\text{Y-ZrO}_2/\text{YZ3-A7/Y-ZrO}_2$  laminate, which displayed severe delamination under bending, was considered to originate from the contribution of residual stresses and strong three-layer  $\text{ZrO}_2$ -containing matrices. This severe delamination, rarely seen in ceramics, can be an effective toughening mechanism to prevent ceramics from brittle fracture. From the result of this laminate, three approaches to promote extended delamination were proposed. A  $\text{LaPO}_4$ -containing  $\text{ZrO}_2$  laminate also has demonstrated a satisfactory strength and damage-tolerance. Most of the  $\text{YPO}_4$ - and  $\text{LaPO}_4$ -containing  $\text{ZrO}_2$  laminates displayed brittle fracture. The different fracture behaviors were discussed.

Results of fiber pushout tests and a double-shear test are also discussed in chapter 6. The different pushout responses, with changing coating thickness for two  $\text{Al}_2\text{O}_3$ -matrix fiber model composites, were distinguished by attributing them to the residual axial and radial stresses, which were explicitly expressed in the Liang-Hutchinson pushout model. There was a consistent value of interface fracture energy for the  $\text{LaPO}_4$ -coated YAG fiber/ $\text{Al}_2\text{O}_3$  matrix composite, while scattered values were observed for the  $\text{LaPO}_4$ -coated sapphire fiber/ $\text{Al}_2\text{O}_3$

matrix composite. A chemical reaction at the  $\text{LaPO}_4$ /sapphire fiber interface explains the discrepancy in interface fracture energy. The measured interface fracture energy was applied to the debonding criterion for predicting the performance of fiber-reinforced ceramic composites. A similar discussion was made for two  $\text{Y}_3\text{Al}_5\text{O}_{12}$ -matrix fiber model composites. A consistent result for the  $\text{YPO}_4$ /YAG interface fracture energy in two different matrix systems (a  $\text{YPO}_4$ -coated YAG fiber/ $\text{Al}_2\text{O}_3$  matrix system vs a  $\text{YPO}_4$ -coated YAG fiber/ $\text{Y}_3\text{Al}_5\text{O}_{12}$  matrix system) was also explained. In the last chapter 7, conclusions and future work were drawn.

## TABLE OF CONTENTS

<b>CHAPTER 1: INTRODUCTION</b>	1
<b>CHAPTER 2: LITERATURE SURVEY</b>	5
2.1 TOUGHENING MECHANISMS IN CERAMICS	5
2.1.1 Transformation Toughening	5
2.1.2 Microcracking Toughening	7
2.1.3 Particulate Toughening	7
2.1.4 Whisker or Fiber Reinforcement	8
2.2 REVIEW OF CERAMIC FIBER-REINFORCED COMPOSITES	10
2.2.1 Background	10
2.2.2 Criteria For Fabricating Fiber-Reinforced Composites	11
2.2.2.1 Ideal Fiber Qualifications	11
2.2.2.2 Requirements of Ideal Fiber-Reinforced Composites	11
2.2.3 Mode I Failure Criteria for Fiber-Reinforced Composites	12
2.2.3.1 Basic Features	12
2.2.3.2 Matrix Cracking Stress	14
2.2.3.3 Toughness	15
2.2.3.4 Ultimate Strength	16
2.2.4 Mixed Mode Failure Criteria for Fiber-Reinforced Composites	17
2.2.5 Problems Associated with Ceramic Fiber-Reinforced Composites	18
2.3 INTERFACES	19
2.3.1 Interface Nature	19
2.3.1.1 Terminology of Interface	19
2.3.1.2 Interface Bonding	19
2.3.2 Criteria for Interface Debonding and Crack Deflection	21

2.3.2.1	Previous Models .....	22
2.3.2.2	He-Hutchinson-Evans Model .....	23
2.3.2.3	Gupta-Yuan-Martinez Model .....	29
2.3.3	Mechanical Testing of Interfaces .....	29
2.3.3.1	Macromechanical Test .....	30
	(1) Tests on Real Fiber-Reinforced Composites .....	30
	(2) Tests on Simple Systems .....	32
2.3.3.2	Laser Spallation .....	34
2.3.3.3	Fiber Pullout Test .....	34
2.3.3.4	Fiber Pushout Test .....	38
	(1) Marshall-Oliver Model .....	40
	(2) Shear-Lag Model .....	41
	(3) Modified Shear-Lag Model .....	42
	(4) Kerans-Parsatharathy (KP) Model .....	43
	(5) Liang-Hutchinson (LH) Model .....	44
2.4	STATUS OF THE DEVELOPMENT OF TOUGH OXIDE FIBER/OXIDE MATRIX COMPOSITES .....	46
2.4.1	Material Selection .....	47
2.4.2	Oxide Fibers .....	49
2.4.3	Fiber Problems .....	51
2.4.4	Oxide Interfaces and Oxide/Oxide Composites .....	52
2.5	THERMAL RESIDUAL STRESSES .....	56
2.5.1	Background .....	56
2.5.2	Analysis of Thermally Induced Residual Stresses .....	57
2.6	STRONG AND TOUGH CERAMICS WITHOUT REINFORCEMENTS .....	61
2.6.1	Laminated Ceramic Composites .....	61
2.6.2	Fibrous Monolithic and Duplex-Structured Ceramics .....	62

## CHAPTER 3: PROPOSALS FOR INVESTIGATING OXIDE FIBER

/OXIDE MATRIX INTERFACES .....	63
3.1 DEVELOPMENT STRATEGY FOR THIS INVESTIGATION .....	63
3.2 APPLICATION OF THE LIANG-HUTCHINSON FIBER PUSHOUT MODEL ..	66
3.3 A MODE II INTERFACE TEST: A DOUBLE-SHEAR $\Gamma_{II}$ TEST .....	68
3.4 A LAMINATE WITH A FOUR-LAYERED CONFIGURATION .....	70

## CHAPTER 4: EXPERIMENTAL PROCEDURES .....

72

4.1 MATERIAL FABRICATION AND PROPERTY CHARACTERIZATION .....	72
4.1.1 Powder Preparation .....	72
4.1.2 Property Characterization .....	74
4.1.2.1 Material Property .....	74
4.1.2.2 Phase Identification, Chemical Compatibility, and Microstructural Characterization .....	74
4.1.3 Laminate Fabrication .....	75
4.1.3.1 Multilayered Laminates .....	75
(1) Simple Laminate Systems .....	75
(2) Laminates with Different Configurations .....	78
(3) $YPO_4$ - and $LaPO_4$ - Containing $ZrO_2$ Laminates .....	79
4.1.3.2 Sandwich and Double-Sandwich Specimens .....	80
4.2 MECHANICAL EVALUATION .....	81
4.2.1 Mechanical Evaluation of Laminated Ceramic Composites .....	81
(1) Simple Laminate Systems .....	81
(2) Laminates with Different Configurations .....	82
(3) $YPO_4$ - and $LaPO_4$ - Containing $ZrO_2$ Laminates .....	83
4.2.2 Interface Mechanical Tests .....	83
4.2.2.1 Double-Shear Testing .....	83

(1) Sample Preparation .....	83
(2) Test Procedures .....	83
4.2.2.2 Mode-I and Mixed-Mode Interface Testing .....	84
(1) Formulation of the DCDC Test Method .....	84
(2) Formulation of the Mixed-Mode Interface Testing .....	85
4.2.2.3 Pushout Tests of Fiber Model Systems .....	86
(1) Sample Preparation .....	86
(2) Pushout Test Procedure .....	88

<b>CHAPTER 5: RESULTS .....</b>	<b>90</b>
5.1 MATERIAL PROPERTIES AND MICROSTRUCTURAL EVALUATION .....	90
5.1.1 Material Properties of Single phase $\text{YPO}_4$ .....	90
5.1.2 Phase Identification and Chemical Compatibility .....	91
5.1.3 Microstructure of Laminated Composites .....	98
(1) Simple Laminate Systems .....	98
(2) Laminates with Different Configurations .....	104
(3) $\text{YPO}_4$ - and $\text{LaPO}_4$ - Containing $\text{ZrO}_2$ Laminates .....	104
5.1.4 Coefficients of Thermal Expansion .....	108
5.2 MECHANICAL EVALUATION .....	111
5.2.1 Indentation Testing .....	111
5.2.2 Flexural Testing .....	112
(1) Simple Laminate Systems .....	112
(2) Laminates with Different Configurations .....	117
(3) $\text{YPO}_4$ - and $\text{LaPO}_4$ - Containing $\text{ZrO}_2$ Laminates .....	118
5.2.3 Interface Mechanical Testing .....	126
5.2.3.1 Double-Shear Testing of a $\text{YPO}_4/\text{Y}_3\text{Al}_5\text{O}_{12}$ System .....	126
5.2.3.2 Mode-I and Mixed-Mode Interface Testing .....	129

5.2.4	Pushout Tests of Fiber Model Systems .....	129
5.2.4.1	Al <sub>2</sub> O <sub>3</sub> -Matrix Model Systems .....	129
(1)	Fiber Pushout Curves .....	129
(2)	Calculation of Interfacial Shear Strength .....	130
(3)	Effect of Coating Thickness on Interfacial Shear Strength .....	134
(4)	The Liang and Hutchinson Model for Fiber Pushout .....	135
(5)	Residual Stress Calculation .....	137
(6)	Estimating $\Gamma_i$ .....	137
5.2.4.2	Y <sub>3</sub> Al <sub>5</sub> O <sub>12</sub> -Matrix Model Systems .....	141
<b>CHAPTER 6: DISCUSSION .....</b>		<b>146</b>
6.1	CHEMICAL AND MICROSTRUCTURAL EVALUATION .....	146
6.1.1	Chemical Compatibility .....	146
6.1.2	Microstructure of Laminated Ceramic Composites .....	147
6.2	MECHANICAL EVALUATION OF LAMINATED COMPOSITES .....	148
6.2.1	Simple Laminate Systems .....	148
6.2.2	Laminates with Different Configurations .....	150
6.2.3	YPO <sub>4</sub> - and LaPO <sub>4</sub> - Containing ZrO <sub>2</sub> Laminates .....	150
(1)	The YPO <sub>4</sub> /Y-ZrO <sub>2</sub> /YZ3-A7/Y-ZrO <sub>2</sub> Oxide Laminate .....	150
(2)	Initiation Mechanism of Residual Interlaminar Shear Stress- ....	
	Enhanced Delamination .....	154
(3)	The LaPO <sub>4</sub> /(YCeSr)Z7-A3 Oxide Laminate .....	159
(4)	Residual Stress Effect on the Behaviors of Different Oxide ....	
	Laminates .....	159
6.3	PUSHOUT TESTS OF FIBER MODEL SYSTEMS .....	164
6.3.1	Discussion of Two Al <sub>2</sub> O <sub>3</sub> -Matrix Fiber Model Systems .....	165
6.3.1.1	Debonding and Sliding in the Al <sub>2</sub> O <sub>3</sub> /LaPO <sub>4</sub> /Al <sub>2</sub> O <sub>3</sub> Fiber System .....	165

6.3.1.2	Debonding and Sliding in the YAG/LaPO <sub>4</sub> /Al <sub>2</sub> O <sub>3</sub> Fiber System	..167
6.3.2	Discussion of Two Y <sub>3</sub> Al <sub>5</sub> O <sub>12</sub> -Matrix Fiber Model Systems	..... 171
6.4	COMPARISONS OF INTERFACE PROPERTIES MEASURED BY DIFFERENT MODE-II SHEAR TESTS	..... 174
6.5	WILL OXIDE COMPOSITES FULLFILL THE TARGET GOAL?	..... 176
<b>CHAPTER 7: CONCLUSIONS AND FUTURE WORK</b>		..... 177
7.1	CONCLUSIONS	..... 177
7.2	FUTURE WORK	..... 182
REFERENCES		..... 184
VITA		..... 216
APPENDIX		..... 217



## LIST OF TABLES

Table 1	Tough ceramics .....	9
Table 2	Oxide fiber properties .....	50
Table 3	Previous research on oxide/oxide-related systems with interfaces survivable at elevated temperatures .....	53
Table 4	Slurry formulation for tape casting of different materials .....	77
Table 5	YPO <sub>4</sub> - and LaPO <sub>4</sub> -containing ZrO <sub>2</sub> laminates fabricated .....	80
Table 6	Summary of material systems for fiber pushout tests .....	86
Table 7	Thermal and mechanical properties of YPO <sub>4</sub> and LaPO <sub>4</sub> .....	90
Table 8	Summary of 4-point flexural strengths of single phases and laminates	114
Table 9	Strength and fracture toughness of laminates with different configurations .....	118
Table 10	Summary of YPO <sub>4</sub> - and LaPO <sub>4</sub> -containing ZrO <sub>2</sub> laminated systems .....	125
Table 11	Properties of fibers, matrices, coatings and interlayers .....	127
Table 12	Parameters of interfacial properties extracted from curve-fitting the Liang- Hutchinson model to pushout data for LaPO <sub>4</sub> -coated Al <sub>2</sub> O <sub>3</sub> fiber/Al <sub>2</sub> O <sub>3</sub> ... matrix and YAG fiber/Al <sub>2</sub> O <sub>3</sub> matrix systems .....	142
Table 13	Work-of-fracture values of many types of materials .....	164
Table 14	Comparisons of fiber fracture energy ( $\Gamma_f$ ) and mode II interfacial fracture energy ( $\Gamma_i$ ) between Al <sub>2</sub> O <sub>3</sub> - and YAG-fiber Al <sub>2</sub> O <sub>3</sub> matrix systems with a LaPO <sub>4</sub> coating .....	171
Table 15	Interfacial properties of YPO <sub>4</sub> -coated and LaPO <sub>4</sub> -coated fiber model ..... composites measured by fiber pushout tests .....	173

## LIST OF FIGURES

Fig. 1 Tensile stress-strain curves for ceramic matrix composites; (a) small $\Gamma_i$ , small $\mu$ and (b) small $\Gamma_i$ , large $\mu$ . .....	13
Fig. 2 A schematic illustration of the initial debonding of fibers at the crack front and fiber debonding in the crack wake. ....	21
Fig. 3 Geometry of crack deflection at an interface. After Kendall <sup>(118)</sup> . ....	22
Fig. 4 The displacement of the surface of a crack at a bimaterial interface indicating the shear and opening displacement that accompany most external loading conditions. ....	24
Fig. 5 (a) Crack front debond diagram indicating the range of relative interface fracture energy, $\Gamma_i/\Gamma_2$ , in which debonding occurs in preference to fiber failure. (b) Trends in phase angle at the debond crack with elastic mismatch. After Evans, He, and Hutchinson. <sup>(125)</sup> . ....	26
Fig. 6 Effect of interface orientation on the debonding requirements. After Evans, He, and Hutchinson. <sup>(125)</sup> .....	27
Fig. 7 Composite diagram concerning fiber failure plotted for materials having $\alpha = 0$ . Trajectories of $\Gamma_i$ with $\psi$ that cause either debond deflection into the fiber or debonding without fiber failure are shown. To obtain these results, the kink angle that gave the maximum value of the energy release rate in the fiber was used, and this energy release rate was equal to $\Gamma_f$ . After Evans, He, and Hutchinson. <sup>(125)</sup> .....	28
Fig. 8 (a) and (b) Transverse 3-point bend test. (c) Short beam shear test. ....	31
Fig. 9 Five kinds of mechanical tests on the model sandwich systems for measuring the interfacial properties. ....	33
Fig.10 Schematic diagram of the laser spallation technique. <sup>(135)</sup> .....	35
Fig.11 Schematic illustration of the fiber pullout test. <sup>(32)</sup> In (a) only one end of the fiber is embedded in the matrix whereas in (b) both ends are embedded in the matrix. ....	36

Fig.12 Schematic comparison of different indentation techniques. <sup>(149)</sup> (a) Rounded indenter: bond strength calculated from elastic stress field at debond-initiation. (b) Vickers pyramid indenter: interface friction stress calculated from the depth to which fiber is depressed. (c) Thin-slice pushout: debonding stress and friction stress calculated from the force-displacement curve. ....	39
Fig.13 Schematic diagram of a three-element composite consisting of a central fiber surrounded by two concentric sleeves of the coating and the matrix material. ....	58
Fig.14 Flow chart of developing oxide fiber/oxide matrix composites. ....	64
Fig.15 Screening test by indentation technique and 4-point flexural testing to identify the weakness of an interface. ....	65
Fig.16 Schematic presentation of the fiber pushout test with parameters related to this test. ....	67
Fig.17 Schematic representation of the double-shear $\Gamma_{II}$ test. ....	70
Fig.18 Schematic representation of a simplified laminate with a four-layer configuration. ....	71
Fig.19 Procedures for powder preparation by Pechini method. ....	73
Fig.20 Tape casting procedures for making laminated composites. ....	76
Fig.21 Schematic representation of the set-up for fiber pushout tests. ....	89
Fig.22 XRD of a $\text{LaPO}_4/\text{Y}_3\text{Al}_5\text{O}_{12}$ pellet fired at $1600^\circ\text{C}$ for 6 hours. ....	92
Fig.23 XRD of a $\text{LaPO}_4/\text{LaAl}_{11}\text{O}_{18}$ pellet fired at $1600^\circ\text{C}$ for 3 hours. ....	93
Fig.24 XRD results for an $\text{Al}_2\text{O}_3/\text{LaPO}_4$ pellet fired at $1550^\circ\text{C}$ for 6 hours (bottom) and subsequently fired at $1600^\circ\text{C}$ for 6 hours (top). ....	93
Fig.25 Scanning electron micrographs of a single-crystal $\text{Al}_2\text{O}_3$ fiber ( $A_f$ )/ $\text{Al}_2\text{O}_3$ matrix (A) system having $\text{LaPO}_4$ (LP) as an interlayer. (a) sintered at $1550^\circ\text{C}$ for 6 hours and (b) sintered at (a) condition and subsequently fired at $1600^\circ\text{C}$ for 6 hours. ....	94
Fig.26 Corresponding EDS spectra taken from the reaction zones indicated as (i) to (iv) in Fig. 20(b) between the $\text{Al}_2\text{O}_3$ matrix and $\text{LaPO}_4$ interlayer. ....	95

Fig.27 XRD of a $\text{YPO}_4/\text{Al}_2\text{O}_3$ pellet fired at $1550^\circ\text{C}$ for 3 hours. ....	96
Fig.28 XRD of a $\text{YPO}_4/\text{Y}_3\text{Al}_5\text{O}_{12}$ pellet fired at $1600^\circ\text{C}$ for 3 hours. ....	96
Fig.29 XRD results of $\text{Y-ZrO}_2$ , $\text{YPO}_4/\text{Y-ZrO}_2$ (50 vol/50 vol) and $\text{LaPO}_4/\text{Y-ZrO}_2$ (50 vol/50 vol) pellets fired at $1550^\circ\text{C}$ for 3 hours. ....	97
Fig.30 Optical micrographs of four as-fabricated laminates: (a) $\text{LaPO}_4/\text{Al}_2\text{O}_3$ hot pressed at $1300^\circ\text{C}$ for 3 hours; (b) $\text{LaPO}_4/\text{Y}_3\text{Al}_5\text{O}_{12}$ , (c) $\text{LaPO}_4/\text{LaAl}_{11}\text{O}_{18}$ , and (d) $\text{YPO}_4/\text{Y}_3\text{Al}_5\text{O}_{12}$ hot pressed at $1600^\circ\text{C}$ for 3 hours. ....	99
Fig.31 Scanning electron micrographs of four as-fabricated laminates: (a) $\text{LaPO}_4/\text{Al}_2\text{O}_3$ hot pressed at $1300^\circ\text{C}$ for 3 hours; (b) $\text{LaPO}_4/\text{Y}_3\text{Al}_5\text{O}_{12}$ , (c) $\text{LaPO}_4/\text{LaAl}_{11}\text{O}_{18}$ , and (d) $\text{YPO}_4/\text{Y}_3\text{Al}_5\text{O}_{12}$ hot pressed at $1600^\circ\text{C}$ for 3 hours. ....	101
Fig.32 Optical micrographs of hot-pressed $\text{YPO}_4/\text{Y}_3\text{Al}_5\text{O}_{12}$ laminate after manual fracture: (a) cross section of fracture surface and (b) fracture surface. ....	103
Fig.33 Scanning electron micrographs of the fractured bend bars. (a) a $\text{YPO}_4(1)/\text{Y}_3\text{Al}_5\text{O}_{12}(1)$ laminate, (b) a $\text{YPO}_4(1)/\text{Y}_3\text{Al}_5\text{O}_{12}(3)$ laminate, and (c) $\text{YPO}_4/\text{Y}_3\text{Al}_5\text{O}_{12}/\text{Al}_2\text{O}_3/\text{Y}_3\text{Al}_5\text{O}_{12}$ laminate. These laminates were hot pressed at $1600^\circ\text{C}$ for 3 hours. The numbers in the brackets indicate the number of tapes applied in the stacking sequence. ....	105
Fig.34 Scanning electron micrograph of a $\text{YPO}_4/\text{Y-ZrO}_2/30 \text{ vol}\% \text{ Y-ZrO}_2\text{-}70 \text{ vol}\% \text{ Al}_2\text{O}_3/\text{Y-ZrO}_2$ laminate showing three kinds of laminar layers. This laminate was hot pressed at $1550^\circ\text{C}$ for 2 hours. ....	106
Fig.35 Transmission electron micrograph of a $\text{YPO}_4$ layer in the $\text{YPO}_4/\text{Y-ZrO}_2/30 \text{ vol}\% \text{ Y-ZrO}_2\text{-}70 \text{ vol}\% \text{ Al}_2\text{O}_3/\text{Y-ZrO}_2$ laminate. ....	106
Fig.36 Transmission electron micrograph of a $\text{Y-ZrO}_2$ layer in the $\text{YPO}_4/\text{Y-ZrO}_2/30 \text{ vol}\% \text{ Y-ZrO}_2\text{-}70 \text{ vol}\% \text{ Al}_2\text{O}_3/\text{Y-ZrO}_2$ laminate. ....	107
Fig.37 Transmission electron micrograph of a $\text{YZ3-A7}$ layer in the $\text{YPO}_4/\text{Y-ZrO}_2/30 \text{ vol}\% \text{ Y-ZrO}_2\text{-}70 \text{ vol}\% \text{ Al}_2\text{O}_3 (\text{YZ3-A7})/\text{Y-ZrO}_2$ laminate. ....	107

Fig.38 Transmission electron micrograph of a crack close to a Y-ZrO <sub>2</sub> /YZ3-A7 interface in the Y-ZrO <sub>2</sub> layer of a 30 vol% Y-ZrO <sub>2</sub> -70 vol% Al <sub>2</sub> O <sub>3</sub> layer in the YPO <sub>4</sub> /Y-ZrO <sub>2</sub> /30 vol% Y-ZrO <sub>2</sub> -70 vol% Al <sub>2</sub> O <sub>3</sub> (YZ3-A7)/Y-ZrO <sub>2</sub> laminate. ....	109
Fig.39 Transmission electron micrograph around the YPO <sub>4</sub> /Y-ZrO <sub>2</sub> interface of the YPO <sub>4</sub> /Y-ZrO <sub>2</sub> /30 vol% Y-ZrO <sub>2</sub> -70 vol% Al <sub>2</sub> O <sub>3</sub> /Y-ZrO <sub>2</sub> laminate. ....	109
Fig.40 Thermal expansion of YPO <sub>4</sub> in this study compared with literature values of LaPO <sub>4</sub> <sup>(48)</sup> and single crystal Y <sub>3</sub> Al <sub>5</sub> O <sub>12</sub> (YAG) <sup>(235)</sup> .....	110
Fig.41 Thermal expansion of LaAl <sub>11</sub> O <sub>18</sub> as measured by dilatometry. ....	110
Fig.42 Enlarged micrograph of interfacial delamination in the indented laminate shown in Fig. 28(c) (marked by arrows). ....	111
Fig.43 SEM micrographs of indentation crack patterns in a YPO <sub>4</sub> /Y-ZrO <sub>2</sub> /30 vol% Y-ZrO <sub>2</sub> -70 vol% Al <sub>2</sub> O <sub>3</sub> /Y-ZrO <sub>2</sub> laminate. Indents were oriented at (a) 0°/90° and (b) 45° relative to the layer length direction. ....	113
Fig.44 Scanning electron micrograph of interfacial delamination in a notched LaPO <sub>4</sub> /LaAl <sub>11</sub> O <sub>18</sub> laminate after a flexural test. ....	115
Fig.45 Load-deflection curves for YPO <sub>4</sub> /Y <sub>3</sub> Al <sub>5</sub> O <sub>12</sub> laminate under 4-pt flexural testing. Curve A was measured for a bar with a ground tensile surface and curve B for a bar with a notched tensile surface. Specimen dimensions were 25 mm × 2.0 mm × 1.9 mm. ....	115
Fig.46 Optical micrographs of bars after flexural testing; (a) YPO <sub>4</sub> /Y <sub>3</sub> Al <sub>5</sub> O <sub>12</sub> laminate and (b) single phase Y <sub>3</sub> Al <sub>5</sub> O <sub>12</sub> specimen with ground tensile surfaces, and (c) SEM micrograph of YPO <sub>4</sub> /Y <sub>3</sub> Al <sub>5</sub> O <sub>12</sub> laminate with a notch on the tensile surface. These bars were annealed in air at 1450°C for 6 hours before flexural testing. ....	116
Fig.47 Load vs displacement curves of a YPO <sub>4</sub> /Y-ZrO <sub>2</sub> /30 vol% Y-ZrO <sub>2</sub> -70 vol% Al <sub>2</sub> O <sub>3</sub> /Y-ZrO <sub>2</sub> laminate tested in 4-point flexure. ....	119

Fig.48 (a) Optical and (b) SEM micrographs showing the side surfaces of a $\text{YPO}_4/\text{Y-ZrO}_2/$ 30 vol% $\text{Y-ZrO}_2$ -70 vol% $\text{Al}_2\text{O}_3/\text{Y-ZrO}_2$ laminate after 4-point flexural testing. .....	120
Fig.49 Load vs displacement curves of a $\text{LaPO}_4/70$ vol% $(\text{YCeSr})\text{ZrO}_2$ -30 vol% $\text{Al}_2\text{O}_3/$ laminate tested in 4-point flexure. ....	121
Fig.50 SEM micrograph showing the side surfaces of a $\text{LaPO}_4/70$ vol% $(\text{YCeSr})\text{ZrO}_2$ -30 vol% $\text{Al}_2\text{O}_3$ laminate after 4-point flexural testing. ....	121
Fig.51 Load vs displacement curves of a $\text{LaPO}_4/70$ vol% $(\text{YCeSr})\text{ZrO}_2$ -30 vol% mullite/ $\text{Al}_2\text{O}_3/70$ vol% $(\text{YCeSr})\text{ZrO}_2$ -30 vol% mullite laminate tested in 4-point flexure. .....	123
Fig.52 SEM micrograph showing the side surfaces of a $\text{LaPO}_4/70$ vol% $(\text{YCeSr})\text{ZrO}_2$ -30 vol% mullite/ $\text{Al}_2\text{O}_3/70$ vol% $(\text{YCeSr})\text{ZrO}_2$ -30 vol% mullite laminate after 4-point flexural testing. ....	123
Fig. 53 SEM micrographs showing the side surfaces of (a) a 70 vol% $\text{YPO}_4$ -30 vol% $\text{Y-ZrO}_2$ /70 vol% $(\text{YCeSr})\text{-ZrO}_2$ -30 vol% $\text{Al}_2\text{O}_3/\text{Al}_2\text{O}_3/70$ vol% $(\text{YCeSr})\text{-ZrO}_2$ -30 vol% $\text{Al}_2\text{O}_3$ laminate and (b) a 70 vol% $\text{YPO}_4$ -30 vol% $\text{Y-ZrO}_2/70$ vol% $(\text{YCeSr})\text{-ZrO}_2$ -30 vol% $\text{Al}_2\text{O}_3$ laminate after 4-point flexural tests .....	124
Fig.54 A load vs displacement curve for a double sandwich specimen of a $\text{YPO}_4/\text{Y}_3\text{Al}_5\text{O}_{12}$ system under the double-shear $\Gamma_{II}$ test. ....	126
Fig.55 (a) Optical micrograph of a tested double-shear specimen and (b) SEM micrograph of the side view of the interlayer region (arrows indicate the notch positions) of a double-sandwiched $\text{YPO}_4/\text{Y}_3\text{Al}_5\text{O}_{12}$ specimen. ....	128
Fig.56 Typical pushout curves for $\text{LaPO}_4$ -coated (a) $\text{Al}_2\text{O}_3$ fiber/ $\text{Al}_2\text{O}_3$ matrix and (b) YAG fiber/ $\text{Al}_2\text{O}_3$ matrix systems. ....	131
Fig.57 SEM micrographs of pushed-out fibers for (a) $\text{YPO}_4$ -coated YAG fiber/ $\text{Y}_3\text{Al}_5\text{O}_{12}$ matrix system and (b) $\text{LaPO}_4$ -coated YAG fiber/ $\text{Y}_3\text{Al}_5\text{O}_{12}$ matrix system. ....	132

Fig.58	Variation of peak load ( $p_p$ ) during pushout as a function of embedded fiber length ( $L$ ) for: LaPO <sub>4</sub> -coated (a) Al <sub>2</sub> O <sub>3</sub> fiber/Al <sub>2</sub> O <sub>3</sub> matrix system and (b) YAG fiber/Al <sub>2</sub> O <sub>3</sub> matrix system. Best fit curves are used to extract a shear strength for the interface using both shear-lag and linear models. ....	133
Fig.59	Variation of interfacial shear strength ( $\tau_d$ ) as a function of coating thickness for: LaPO <sub>4</sub> -coated (a) Al <sub>2</sub> O <sub>3</sub> fiber/Al <sub>2</sub> O <sub>3</sub> matrix system and (b) YAG fiber/Al <sub>2</sub> O <sub>3</sub> matrix system. ....	134
Fig.60	Calculated residual stress distribution as a function of coating thickness for both the Al <sub>2</sub> O <sub>3</sub> and YAG fiber systems having Al <sub>2</sub> O <sub>3</sub> as the matrix: (a) Axial stress in the fiber. (b) Radial stress acting across the fiber/coating interface. ....	138
Fig.61	Variations of peak debond stress just before complete debonding ( $P_p$ ) and sliding stress immediately following complete debonding ( $P_l$ ) for the LaPO <sub>4</sub> -coated Al <sub>2</sub> O <sub>3</sub> fiber /Al <sub>2</sub> O <sub>3</sub> matrix system as a function of embedded fiber length ( $L$ ); (a) 6.5 $\mu$ m coating thickness (b) 16 $\mu$ m coating thickness. ....	139
Fig.62	Variations of peak debond stress just before complete debonding ( $P_p$ ) and sliding stress immediately following complete debonding ( $P_l$ ) for the LaPO <sub>4</sub> -coated YAG fiber/Al <sub>2</sub> O <sub>3</sub> matrix system as a function of embedded fiber length ( $L$ ); (a) 2 $\mu$ m coating thickness, (b) 9 $\mu$ m coating thickness. ....	140
Fig.63	(a) A typical fiber pushout curve and (b) SEM micrograph of a pushed-out fiber for the YAG fiber/YPO <sub>4</sub> coating/Y <sub>3</sub> Al <sub>5</sub> O <sub>12</sub> matrix model composite. ....	143
Fig.64	Estimating $\Gamma_{II}$ by curve-fitting Liang-Hutchinson equations to the experimental data for (a) the YPO <sub>4</sub> -coated YAG fiber/Y <sub>3</sub> Al <sub>5</sub> O <sub>12</sub> matrix and (b) the LaPO <sub>4</sub> -coated YAG fiber/Y <sub>3</sub> Al <sub>5</sub> O <sub>12</sub> matrix composites. ....	145
Fig.65	Initiation mechanism of interfacial delamination occurring in the YPO <sub>4</sub> /Y-ZrO <sub>2</sub> /YZ3A7/Y-ZrO <sub>2</sub> laminate. (a) a simplified laminate, (b) and (c) applied stress distribution, (d) the pre-existing residual stress located at weak interfaces, and (e) superposition of the applied and residual shear stresses. ....	156

Fig.66 Schematical presentation of residual interlaminar shear-enhanced initiation mechanism of interfacial delamination occurred in the $\text{YPO}_4/\text{Y-ZrO}_2/\text{YZ3-A7/Y-ZrO}_2$ laminate. ....	158
Fig.67 Variation of average sliding stress as a function of interfacial coating thickness for both the $\text{LaPO}_4$ -coated $\text{Al}_2\text{O}_3$ fiber/ $\text{Al}_2\text{O}_3$ matrix and YAG fiber/ $\text{Al}_2\text{O}_3$ matrix systems. ....	166
Fig.68 SEM micrographs of the interface region for $\text{LaPO}_4$ -coated (a) $\text{Al}_2\text{O}_3$ fiber/ $\text{Al}_2\text{O}_3$ matrix and (b) YAG fiber/ $\text{Al}_2\text{O}_3$ matrix systems. Arrows mark the reaction product at the fiber/coating interface of $\text{Al}_2\text{O}_3$ fiber system. The reaction product is obvious at the coating/matrix interfaces for both fiber systems. ....	168



## CHAPTER 7: CONCLUSIONS AND FUTURE WORK

### 7.1 CONCLUSIONS

The investigation and development of oxide fiber/oxide matrix systems in this work proceeded as follows: material selection/design → powder processing → studies of chemical compatibility and physical stability → densification techniques → macromechanical and micromechanical testing → proposing mechanics methodologies → microstructural evaluation.

#### Material Properties

Young's modulus, Poisson's ratio, Vickers hardness, fracture toughness, and 4-pt flexural strength of sintered  $\text{YPO}_4$  were measured to be 152 GPa, 0.28, 5.9 GPa, 1.1  $\text{MPa}\cdot\text{m}^{1/2}$ , and  $\sim 75$  MPa, respectively. The linear thermal expansion coefficients for  $\text{YPO}_4$  were  $7.7 \times 10^{-6}/^\circ\text{C}$  at  $200^\circ\text{C}$ ,  $8.6 \times 10^{-6}/^\circ\text{C}$  at  $600^\circ\text{C}$ , and  $9.3 \times 10^{-6}/^\circ\text{C}$  at  $1000^\circ\text{C}$ , with an average over this temperature range of  $8.6 \times 10^{-6}/^\circ\text{C}$ . The linear thermal expansion coefficients for  $\text{LaAl}_{11}\text{O}_{18}$  were  $8.8 \times 10^{-6}/^\circ\text{C}$  at  $200^\circ\text{C}$ ,  $10.0 \times 10^{-6}/^\circ\text{C}$  at  $600^\circ\text{C}$ , and  $10.8 \times 10^{-6}/^\circ\text{C}$  at  $1000^\circ\text{C}$ , with an average over this temperature range of  $10.0 \times 10^{-6}/^\circ\text{C}$ .

#### Chemical Compatibility

Identification of chemical compatibility was executed on several kinds of oxide systems. These results indicated that there were no chemical reactions between  $\text{LaPO}_4$  and  $\text{Y}_3\text{Al}_5\text{O}_{12}$ , between  $\text{LaPO}_4$  and  $\text{LaAl}_{11}\text{O}_{18}$ , between  $\text{LaPO}_4$  and yttria-stabilized  $\text{ZrO}_2$  (Y- $\text{ZrO}_2$ ), between  $\text{YPO}_4$  and  $\text{Y}_3\text{Al}_5\text{O}_{12}$ , and between  $\text{YPO}_4$  and Y- $\text{ZrO}_2$ , up to at least  $1600^\circ\text{C}$ . There are chemical reactions between  $\text{LaPO}_4$  and  $\text{Al}_2\text{O}_3$  to form  $\text{LaAl}_{11}\text{O}_{18}$  and between

YPO<sub>4</sub> and Al<sub>2</sub>O<sub>3</sub> to form Y<sub>3</sub>Al<sub>5</sub>O<sub>12</sub>, as demonstrated by sintering experiments at 1550°C. The chemical reactions were formulated.

### **Multilayered Oxide Laminates**

Fabricating multilayered oxide laminates by the tape-casting technique is a cost-effective route for studying interface behavior, without the use of expensive fibers. Three kinds of multilayered oxide laminates were fabricated here: simple laminate systems, laminates with different configurations, and the YPO<sub>4</sub>- and LaPO<sub>4</sub>-containing ZrO<sub>2</sub> laminates.

### Microstructural and Structural Stability

Morphological instability was not observed at interfaces in all kinds of oxide laminates. These interfaces included LaPO<sub>4</sub>/Y<sub>3</sub>Al<sub>5</sub>O<sub>12</sub>, LaPO<sub>4</sub>/LaAl<sub>11</sub>O<sub>18</sub>, LaPO<sub>4</sub>/Y-ZrO<sub>2</sub>, LaPO<sub>4</sub>/Y<sub>3</sub>Al<sub>5</sub>O<sub>12</sub>, LaPO<sub>4</sub>/Y-ZrO<sub>2</sub>, and Al<sub>2</sub>O<sub>3</sub>/Y<sub>3</sub>Al<sub>5</sub>O<sub>12</sub> interfaces.

Residual stresses in laminates due to the thermal expansion difference between constituents played an important role in structural stability of laminates. Simple laminate systems and laminates with different configurations were structurally stable. However, laminate disintegration occurred in YPO<sub>4</sub>/Y-ZrO<sub>2</sub> and LaPO<sub>4</sub>/Y-ZrO<sub>2</sub> laminates. Other laminate structures in the YPO<sub>4</sub>- and LaPO<sub>4</sub>-containing ZrO<sub>2</sub> laminates remained stable. The structural stability of laminates relied on several factors: material selection, residual stress state (tensile vs compressive) and magnitude, and symmetrical stacking to prevent from distortion.

### Mechanical Performance

The indentation technique has been applied to identify qualitatively the interface weakness in bonding. Indent-induced radial cracks propagated across interfaces of

LaPO<sub>4</sub>/Al<sub>2</sub>O<sub>3</sub>, LaPO<sub>4</sub>/Y<sub>3</sub>Al<sub>5</sub>O<sub>12</sub>. Limited interface delamination occurred in the LaPO<sub>4</sub>/LaAl<sub>11</sub>O<sub>18</sub> and YPO<sub>4</sub>/Y<sub>3</sub>Al<sub>5</sub>O<sub>12</sub> systems. Extended interface delamination occurred in the YPO<sub>4</sub>/Y-ZrO<sub>2</sub>/30 vol% Y-ZrO<sub>2</sub>-70 vol% Al<sub>2</sub>O<sub>3</sub> (YZ3-A7)/Y-ZrO<sub>2</sub> laminate.

Four-point fractural testing has also been used to evaluate the oxide laminates. The notched LaPO<sub>4</sub>/Y<sub>3</sub>Al<sub>5</sub>O<sub>12</sub> and YPO<sub>4</sub>/Y<sub>3</sub>Al<sub>5</sub>O<sub>12</sub> laminates in the simple laminate systems displayed interface delamination, while others fractured in a brittle nature. Without a notch, all the simple laminate systems fractured catastrophically. Although there was a four-fold increase in fracture toughness with components in the laminated form ( $\sim 4 \text{ MPa}\cdot\text{m}^{1/2}$ ) as compared with their single phase materials ( $\sim 1 \text{ MPa}\cdot\text{m}^{1/2}$ ), the laminates with different configurations displayed a brittle fracture during strength measurements. Non-brittle fracture was displayed in the YPO<sub>4</sub>/Y-ZrO<sub>2</sub>/YZ3-A7/Y-ZrO<sub>2</sub>, LaPO<sub>4</sub>/70 vol% doped-ZrO<sub>2</sub>-30 vol% Al<sub>2</sub>O<sub>3</sub>, and LaPO<sub>4</sub>/70 vol% doped ZrO<sub>2</sub>-30 vol% mullite/Al<sub>2</sub>O<sub>3</sub>/70 vol% doped ZrO<sub>2</sub>-30 vol% mullite laminates. All oxide laminates had a 4-point strength between 100 and 250 MPa, except for the YPO<sub>4</sub>/Y-ZrO<sub>2</sub>/YZ3-A7/Y-ZrO<sub>2</sub> laminate. This laminate possessed high strength (358 and 392 MPa) and work-of-fracture (8.2 and 10 kJ/m<sup>2</sup>).

An oxide laminate without reinforcements behaved like strong and tough, fiber-reinforced, ceramic composites. This YPO<sub>4</sub>/Y-ZrO<sub>2</sub>/YZ3-A7/Y-ZrO<sub>2</sub> laminate was constructed in a four-layered configuration which combined the three-layered ZrO<sub>2</sub>-containing matrix separated by weak YPO<sub>4</sub> layers. During bending fracture, extended interface delamination was located at YPO<sub>4</sub>/Y-ZrO<sub>2</sub> interfaces which dissipated the applied work. The three-layered matrix layers which remained un-broken continued to bear loads. This interface delamination did not mean that the YPO<sub>4</sub>/Y-ZrO<sub>2</sub> interface was inherently weak. Actually the interface was weakened by extra driving forces provided by residual stress. A possible mechanism to explain this fracture behavior was proposed as the residual, interlaminar shear stress-induced, interface delamination. Three approaches on how this mechanism operates were suggested. They include increasing the laminate strength, decreasing the interface debond strength, and adjusting the residual interlaminar shear stress.

Although the  $\text{YPO}_4/\text{ZrO}_2$  interface has been shown to be a promising weak interface in the  $\text{YPO}_4/\text{Y-ZrO}_2/\text{YZ3-A7/Y-ZrO}_2$  laminate system, results from other laminates in the  $\text{YPO}_4$ - and  $\text{LaPO}_4$ -containing systems under bending tests predicted that the bonding of  $\text{YPO}_4/\text{ZrO}_2$  and  $\text{LaPO}_4/\text{ZrO}_2$  interfaces is not weak. Thus, the discovery of a better weak interphase to modify the oxide fiber/oxide matrix composites still remains to be achieved.

## **Interface Mechanical Tests**

Micromechanical testing (e.g. fiber pushout test) of fiber-reinforced composites has been an important tool in understanding the interface properties of these composites, if valuable fibers are available and attainable. In this work, single crystal sapphire and YAG fibers were used in the form of fiber model systems to study the interface properties. A methodology to extract the interface properties from the pushout data was developed. A test methodology combining the double-shear test with the fracture mechanics concept also has been proposed to evaluate interface. In this test, no expensive fibers are needed.

### Fiber Pushout Tests

#### (i) Effect of Coating Thickness on Interface Properties

From the fiber pushout testing on the fiber model systems, much useful information was obtained. The effect of the  $\text{LaPO}_4$  coating thickness on the mechanical properties of the fiber/matrix interface was evaluated for both  $\text{LaPO}_4$ -coated alumina and YAG fibers embedded in an alumina matrix. The different thermal and elastic properties of the constituents resulted in different distributions of residual stresses for each fiber system. The  $\text{LaPO}_4$  fiber coating played a key role by promoting debonding, protecting the fibers, and by providing a compliant buffer that altered the resulting residual stress distribution at the interface. As a consequence, the mechanics of debonding and sliding were affected by the absolute coating thickness. Changes in interfacial shear strength with  $\text{LaPO}_4$  coating

thickness for two  $\text{Al}_2\text{O}_3$ -matrix systems (Fig. 59) were rationalized by estimating the change in residual stresses. An increase in the coating thickness was found to decrease the interfacial shear strength required for debonding in the  $\text{LaPO}_4$ -coated  $\text{Al}_2\text{O}_3$  fiber/ $\text{Al}_2\text{O}_3$  matrix model system, while a slight increase was observed for the  $\text{LaPO}_4$ -coated YAG fiber/ $\text{Al}_2\text{O}_3$  matrix model system. These experimentally observed changes in the interfacial shear strength are in accord with what was predicted by the Liang and Hutchinson pushout model.

The mode II interfacial fracture energy of the  $\text{LaPO}_4$ -coated  $\text{Al}_2\text{O}_3$  fiber/ $\text{Al}_2\text{O}_3$  matrix system was found to vary with coating thickness. It was noted previously that there was a reaction product that formed along both the matrix and fiber sides of the  $\text{LaPO}_4$ /alumina interface, Fig. 68(a). Interactions between the debond and the reaction product resulted in a tortuous fracture path and a related increase in the fracture toughness of the interface. There was no detectable reaction between the YAG fiber and  $\text{LaPO}_4$  coating in the  $\text{Al}_2\text{O}_3$ -matrix system (Fig. 68(b)), resulting in a consistent value of the interfacial fracture energy with coating thickness for the  $\text{LaPO}_4$ -coated YAG fiber/ $\text{Al}_2\text{O}_3$  matrix system.

#### (ii) Applying the Liang-Hutchinson Pushout Model

An experimental methodology was presented for extracting the key interfacial parameters from pushout tests on fiber reinforced model systems. The methodology utilized the pushout model developed by Liang and Hutchinson to curve-fit results of pushout tests conducted on specimens of varying coating thickness. This LH model was found to mechanistically rationalize the effect of coating thickness on the mechanical properties of the fiber/coating interface, leading to a detailed understanding of the mechanics of fiber debonding and sliding. The methodology provided a measure of the pure mode II fracture toughness of the interface. Using the LH model and the experimental methodology described herein, coatings can be designed to provide a broad range of debonding and sliding properties.

(iii) Al<sub>2</sub>O<sub>3</sub>-Matrix Fiber Model Systems

Mode II interface properties of the LaPO<sub>4</sub>-coated Al<sub>2</sub>O<sub>3</sub> fiber/Al<sub>2</sub>O<sub>3</sub> matrix and YAG fiber/Al<sub>2</sub>O<sub>3</sub> matrix systems (i.e. the Al<sub>2</sub>O<sub>3</sub>-matrix systems) as a function of coating thickness were obtained by the fiber pushout test as (Table 11): 11-47 and 16.5 J/m<sup>2</sup> for mode II fracture energy, 0.20-0.27 and 0.18 for coefficient of friction, 34-40 and 34 MPa for tensile residual axial stress in the fiber, 170-230 and 400-460 MPa for clamping stress, and 30-60 (compressive) and 20-30 (tensile) MPa for residual radial stress acting at the fiber/coating interface, 90-130 and 90-110 MPa for shear debond strength, and 70-80 and 80-90 MPa for frictional strength, respectively.

(iv) Y<sub>3</sub>Al<sub>5</sub>O<sub>12</sub>-Matrix Fiber Model Systems

Mode II interface properties of the YPO<sub>4</sub>- and LaPO<sub>4</sub>-coated Y<sub>3</sub>Al<sub>5</sub>O<sub>12</sub>-matrix systems were also measured by the fiber pushout test as (Table 15): 22 and 14.5 J/m<sup>2</sup> for mode II fracture energy, 0.27 and 0.23 for coefficient of friction, 324 and 290 MPa for tensile residual axial stress in the fiber, 209 and 327 MPa for clamping stress, 147 and 157 MPa for tensile residual radial stress acting at the fiber/coating interface, 356 and 484 MPa for asperity pressure, 95 and 102 MPa for shear debond strength, and 71 and 88 MPa for frictional strength, respectively.

A Double-Shear  $\Gamma_{II}$  Test

It is preferable to identify a weak interface between a candidate couple in a simple way. Fiber pushout testing is an important technique, but not a necessary tool at the developing stage. A double-shear  $\Gamma_{II}$  test has been proposed as a simple tool to evaluate the mode II interface properties of the YPO<sub>4</sub>/Y<sub>3</sub>Al<sub>5</sub>O<sub>12</sub> system in the form of a double-sandwich system. The 'force'-conceptualized, double-shear test has been modified to a 'energy'-conceptualized test, after combining with fracture mechanics. This method has the potential to be an easy and executable test for studying mode-II interface properties. The interface properties of the double-sandwich YPO<sub>4</sub>/Y<sub>3</sub>Al<sub>5</sub>O<sub>12</sub> specimen measured by the double-shear

test were:  $3.1 \text{ MPa}\cdot\text{m}^{1/2}$  as the mode II stress intensity factor,  $29.0 \text{ J/m}^2$  for mode II fracture energy, 33 MPa for shear debond strength, and 17 MPa for frictional strength.

A better understanding in evaluating interface bonding in oxide systems has been obtained in  $\text{YPO}_4/\text{Y}_3\text{Al}_5\text{O}_{12}$  and  $\text{LaPO}_4/\text{Y}_3\text{Al}_5\text{O}_{12}$  interfaces. Macromechanical tests by bending of laminates, as well as micromechanical tests by fiber pushout tests of fiber model systems have been conducted. The brittle fracture of these oxide laminates under bending is attributed to high interface fracture energy, interface debonding and frictional strengths, obtained from the fiber pushout test.

Thus, it is concluded that  $\text{YPO}_4/\text{oxide}$  and  $\text{LaPO}_4/\text{oxide}$  interface bonding is not, at this stage, as weak as demonstrated in the graphite/non-oxide and boron nitride/non-oxide interfaces. Although oxide fiber/oxide matrix composites with a weak interphase are highly in demand, strong and tough oxide laminates are recommended as a material for applications in the short-term.